Master Thesis:
”Advanced bioresin development for 3D printing of hydrogel-based soft tissues with applications in regenerative medicine”

Author: Evangelia-Eirini Zeringa (4750306)
Supervisors: Prof. Harrie Weinans & Dr Riccardo Levato

January 2020

Table of Contents

1 Introduction and background information

1.1 Bioprinting
1.2 Hydrogels
1.3 Challenges
1.4 Research questions
1.5 Aim of the study

2 Materials and Methods

2.1 Components of hydrogel bioinks
2.2 Preparation of hydrogel bioinks
2.3 DLP printing system
2.4 Printing optimization of hydrogel bioinks
  2.4.1 Investigation of spatial printing resolution
2.5 Characterization of final optimal hydrogel bioinks
  2.5.1 Crosslinking efficiency
  2.5.2 Mechanical properties of bulk materials
2.6 Design of porous scaffold
2.7 Mechanical characterization of scaffold
2.8 Cell culture
2.9 Bioprinting and post-cell seeding of hydrogel scaffolds
2.10 Cell viability and proliferation studies
  2.10.1 Live/Dead Assay
  2.10.2 Alamar Blue Assay
2.11 Statistical Analysis

3 Results

3.1 Prinitng optimization of hydrogel bioinks
  3.1.1 Development of working curves
  3.1.2 Calculation of critical energy and light penetration depth
  3.1.3 Test cube design print
  3.1.4 Investigation of spatial printing resolution
3.2 Characterization of optimal bioinks
  3.2.1 Crosslinking efficiency
  3.2.2 Mechanical properties of bulk materials
3.3 Successful printing of hydrogel scaffolds
3.4 Mechanical characterization of hydrogel scaffolds
3.5 Cell viability and proliferation tests for bioprinted and post-cell seeded hydrogel scaffolds

3.5.1 Live/Dead Assay
3.5.2 Alamar Blue Assay
4 Discussion
4.1 Choice of resin components
4.2 Printing optimization of hydrogel bioinks
4.3 Characterization of final optimal hydrogel bioinks
4.3.1 Problems with Atum3D printer and re-optimization of bioinks
4.3.2 Crosslinking efficiency
4.3.3 Mechanical properties of bulk materials
4.4 Characterization of scaffolds' mechanical performance
4.4 Characterization of scaffolds' biological performance
5 Conclusions and Future Outlook

Abstract

The synergy of hydrogel processing and 3D printing technologies has paved the way for the development of advanced tissue engineering scaffolds. Hydrogels constitute a promising class of materials for the creation of scaffolds due to their permeable environment, suitable for encapsulation, as well as their tunable chemical and mechanical properties [1]. 3D printing, on the other hand, has immersed as a novel manufacturing technology that allows the creation of three dimensional constructs with pre-determined architecture. Current advancements have enabled also the printing of biomaterials incorporating cells and supporting components creating complex structures that can mimic living tissue characteristics with high accuracy [2]. Stereolithography and particularly, the Digital Light Processing (DLP) technology appears as one of the most auspicious printing techniques for the fast creation of mechanically stable hollow structures. However, the difficulty in developing hydrogel bioinks, which could be used for the fabrication of high resolution complicated architectures with structural integrity, remains a challenge. In the present study, efforts were focused on finding the components that could be used for the creation of an optimal bioink suitable for DLP printing. After deciding on the most promising components, the bioink's optimization in terms of printing resolution was performed taking under consideration the fundamental principles of stereolithography. To achieve this goal, the working curves and all the key parameters, which define a photopolymer's behavior were studied. After the optimization of the resolution, the prospective bioinks were characterized in terms of their crosslinking efficiency and mechanical properties. Consequently, complex porous scaffolds were fabricated from the selected bioinks and mechanically tested. Finally, the encapsulation of cells into the bioinks, as well as, the seeding method were performed for the creation of cell-laden scaffolds, which were also studied through the performance of cell viability and proliferation tests.

Chapter 1

Introduction and background information

1.1 Bioprinting

Additive manufacturing, or otherwise known as 3D printing is one of the most revolutionary technologies of the century driving innovations in multidisciplinary areas [3].

Recent advancements have enabled researchers in the field of biomedical engineering to utilize this concept as a transformative tool for a wide range of applications especially in the area of regenerative medicine and tissue engineering [4].

Particularly, bioprinting refers to the utilization of the 3D printing technology for the fabrication of scaffolds, i.e. three-dimensional constructs that mimic the extracellular matrix (ECM) of human tissues offering cells a platform for adhesion, proliferation and differentiation [5]. These constructs can be used either for clinical applications, as transplantable implants, in order to recover the function of a damaged tissue and organ, or for research applications, as in vitro tissue models, for drug screening and pathology studies [6]. These applications have great importance due to the global shortage of transplantable tissues/organs and the fact that traditional 2D cell cultures and animal models produce results that often fail to be extrapolated for humans [7]. The idea behind the concept of bioprinting and the potential final application can be observed at **Figure 1.1**.

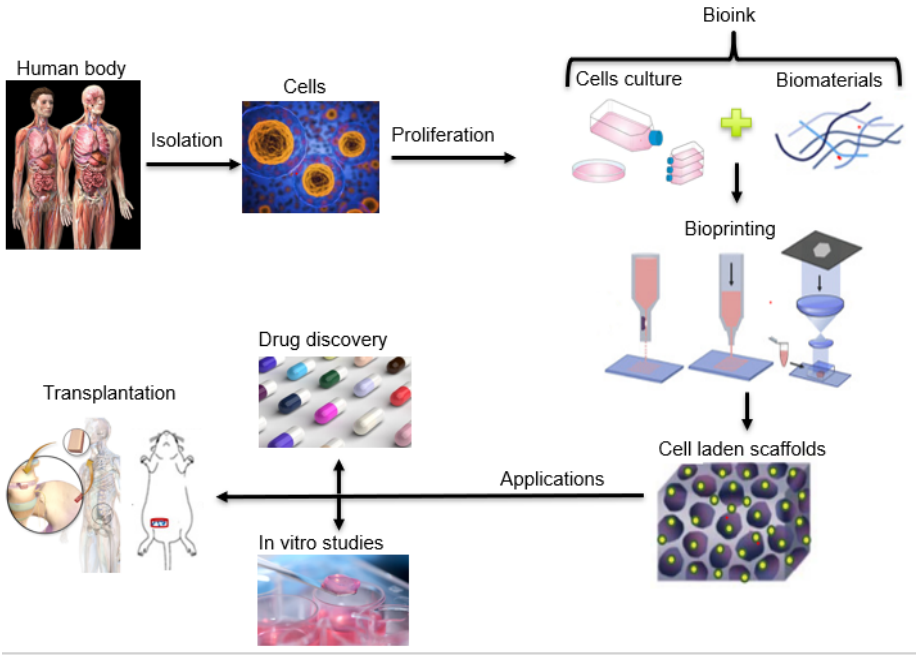

Figure 1.1: Bioprinting process workflow and potential applications.

Since the early 1990's, a great number of conventional methods have been developed for the creation of 3D scaffolds, including gas foaming [8, 9], solvent casting and particulate leaching [10, 11], phase separation [12, 13], freeze drying [14], and electrospinning [15]. However, none of these techniques allow the actual control over the topology and the internal architecture of the structures [16]. On the contrary, 3D printing, assisted by the computer-aided design (CAD) technology, provides not only precision, but also repeatability to the fabrication process of scaffolds [17]. Moreover, medical images from magnetic resonance imaging (MRI) or computed tomography (CT) scans can be utilized to create 3D CAD models which can be printed having patient-specific anatomically correct geometries.

Despite the several successfully reported applications of bioprinting, which prove its feasibility and versatility, there are still many inherent shortcomings that characterize the different available bioprinting techniques. In order to realize these limitations and choose the most suitable option based on the requirements of each research's final product, it is important to understand the working principles of each bioprinting method, which can be generally classified in the following categories:

i) inkjet-based, ii) extrusion-based, iii) laser-assisted and iv) 3D lithography-based bioprinting.

The earliest development of the bioprinting systems originated from the modification of commercially available inkjet printers [18]. These kind of printers have either a thermal or a piezoelectric actuator, which help in the ejection of cell suspension and material drops, through the local increase of temperature or the voltage employment, correspondingly, in order to create of a bubble that drives drops through the nozzle (**Figure 1.2a**). With this technique is difficult to create vertical constructs since the printing head can not generate a continuous flow [5].

To overcome this issue, extrusion-based bioprinting methods utilize a pump (air pressure), or a piston/screw (vertical/rotational mechanical forces) to continuously push the bioink through the syringe tip [19], as can be seen in **Figure 1.2b**. Several materials and cell types can be printed exhibiting a wide range of viscosities and cell densities with this technique. The fact that it constitutes a nozzle-based printing method, as the inkjet one, offers the opportunity for multiple material delivery and has low cost, but at the same time involves the risk of nozzle clogging, as well as, cell damaging due to the shear forces that applied to the cells during printing, rendering the cell viability usually lower than 80% [6].

The laser-assisted bioprinting is based on the principles of Laser Induced Forward Transfer (LIFT) technique [20]. It utilizes a high intensity laser that focuses on a laser-absorbing layer, which is vaporized leading to the creation of a high-pressure bubble that propels the biomaterial underneath towards the collectors substrate in the form of droplets (**Figure 1.2c**) . Since no direct force is applied to the cells, this technique can preserve high cell viability ($>$95%) and has also high resolution (formation of droplets $<$50 μm) [21]. However, it is a method characterized with high-associated cost and low printing speed, while the potential side effects of the laser exposure to cells are not fully understood yet [22].

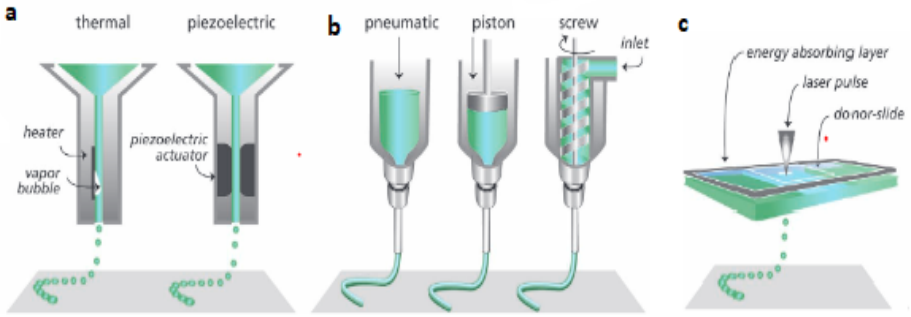

Figure 1.2: (a) Inkjet-based bioprinting method, (b) Extrusion-based bioprinting method, (c) Laser-assisted bioprinting [23].

Stereolithography is a widely used printing method which utilizes light from the UV or visible spectrum in order to selectively crosslink and solidify in a layer-by-layer fashion a photosensitive material following a photochemical process [24]. Particularly, monomers or oligomeres in a liquid state can be cured upon exposure to radiation at specific wavelengths in the presence of a photoinitiator system. Photoinitiators are compounds that upon the absorption of light create reactive species that are able to react with monomeres/oligomeres initiating the polymer chain growth (photopolymerizarion) [25]. From the mid-1980s, where Charles Hull first introduced the term "stereolithography" [26], until today, three different light patterning techniques have been developed: Vector Scanning (SLA), Photo-Mask projection (DLP) and Two-Photon polymerization (2PP).

The SLA is widely used in the majority of commercial printers and it utilizes a laser that is scanned over a vat filled with liquid photosensitive materials leading to the photopolymerization and thus the solidification of the resin creating a 2D pattern. Once a layer has been created the building platform moves downwards in a distance that is equal to the thickness of a layer. In this way fresh uncrosslinked material covers the previously formed 2D pattern and a new layer is built on top of the previous one following a bottom-up construction approach [24]. This procedure is repeated until the final 3D design is printed, as can be observed in **Figure 1.3a**.

The DLP uses also a beam of light to cure polymers, but it allows the irradiation of the entire surface of the photopolymer vat with the help of a digital mirror device (DMD). The DMD has an array of micromirrors, which can rotate independently to control the light to an on and off state, creating in this way a light pattern that is projected on the polymer. An entire layer can be cured at once,

making this printing method, called Digital Light Processing (DLP), faster than any other stereolithography (SLA) method. Each layer attaches to the building plate, which automatically moves upwards in the z-direction allowing the next layer to be crosslinked [28, 29]. This process follows the up-bottom construction approach, as can be seen in **Figure 1.3b** and it continues until all the layers of a CAD design are projected.

At the aforementioned techniques, the absorption of a single photon by singles molecules leads to the initiation of the polymerization process at the surface of the material creating structures with a layer-by-layer approach. However, in the case of the TPP, this initiation is induced by the simultaneously absorption of two photons and can be observed only with laser beams of high intensity [30]. For the accomplishment of this action, the light source of the TPP technique is an infra red (IR) femtosecond laser radiation focused into the volume of a photosensitive hydrogel. The control of the laser's beam at specific directions leads to the direct polymerization at very confined regions within the material [31]. Consequently, the hydrogel precursor solution is crosslinked along the trace of the moving laser focus resulting to the printing of 3D structures, as can be seen in **Figure 1.3c**. This relatively new printing method allows the fabrication of high resolution prints (with features accuracy less than 100 μm), but it can create small size prints (less than 1 mm^3) [32]. Moreover, due to the fact that the polymerization occurs only at the focal point, TPP is an extremely slow process.

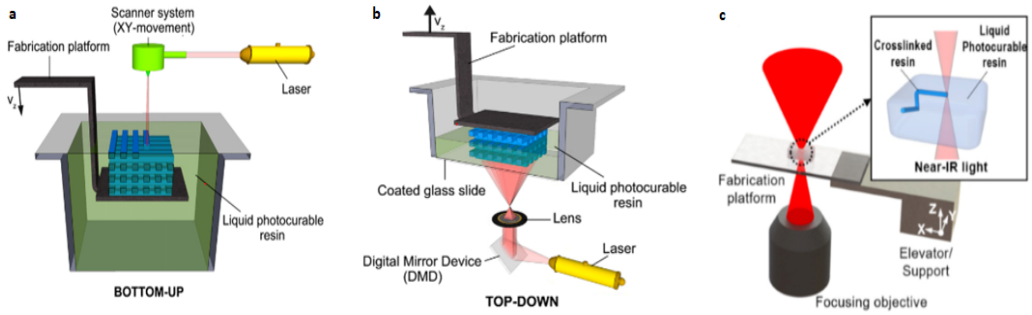

Figure 1.3: 3D Lithography printing methods. (a) Vector scanning (SLA), (b) Photo Mask Projection (DLP), (c) Two - Photon Polymerization (TPP) [27].

1.2 Hydrogels

Hydrogels are three-dimensional networks of hydrophilic polymers crosslinked through covalent bonds or connected via intramolecular and intermolecular attractions [33]. Over the past decade, hydrogels have emerged as one of the most attractive class of materials. They are widely used in the field of bioprinting due to their unique compositional and structural affinity to the native extracellular matrix (ECM), as well as, their enticing framework for cellular survival and proliferation [34]. Particularly, their swelling ability allows them to absorb high water or biological fluids content, expanding readily without dissolving. In this swollen state, most of the hydrogels become softer and more rubbery resembling often the living tissues to a great extent. Moreover, hydrogels' inherent porosity, which facilitates the oxygen, nutrients and metabolic products diffusion within their matrix, as well as, the capability of their direct loading with cells and bioactive molecules, are some of their advantageous characteristics, which justify their utilization as promising candidates for cell transplantation, localized drug depots and scaffolds in the field of tissue engineering [35].

They can be generally divided into two main categories: the natural polymer-based and the synthetic polymer-based hydrogels. Each of these two types has each own set of advantages and drawbacks. Particularly, natural hydrogels are biocompatible due to their intrinsic characteristics of biological recognition, but they are associated with complexities in purification and characterized from poor mechanical strength. On the contrary, synthetic hydrogels have tunable mechanical, as well as, degradation properties, but they exhibit poor cell adhesion [36].

1.3 Challenges

Although at an early stage of development, the synergy of hydrogel processing and 3D bioprinting technologies, is rapidly evolving as a promising tool in the field of tissue engineering, providing researchers the unprecedented ability to create 3D biological architectures [37].

Continuous advancements have been accomplished in creating biofabrication systems with a variety of biomaterials and cells, in an effort to meet specific requirements for the successful development of functional tissues. However, there are still important barriers that overshadow the wide spectrum of hydrogel bioprinting applications and need to be addressed [27].

Many of these challenges lie at key components of the bioprinting process and the complexity of bioink preparation is one of them. Particularly, the appropriate selection of materials that will be used for biofabrication purposes constitute a major concern since they should have appropriate viscosity and printability, should support cell viability and create a substrate with physical and mechanical properties matching these of the native tissue [38]. Naturally-sourced [39] or biomimetic decellularized matrix (dECM) hydrogels [40] lack mechanical strength , while synthetic hydrogels have tunable mechanical properties, but are not suitable for cell attachment [41]. This problem could be resolved with the development of composite or hybrid materials with tunable characteristics that could combine the best of both worlds [42, 43], as well as the further addition of suitable bioactive molecules (like growth factors, peptide ligands, etc) [43–45].

In the present study, after the performance of preliminary experiments, where different mixtures of several components were tested (see Appendix A.1), fish gelatin-methacryloyl (GelMA) and poly(ethylene glycol) diacrylate (PEGDA) appeared to be a promising combination for the development of a hydrogel bioink.

The idea behind the creation of this hybrid was based on the development of a bioink, which could have the advantages of both natural and synthetic hydrogels. Particularly, pure GelMA can provide an optimal biological environment to cells due to its soft hydrated environment and the retaining of RGD cell adhesion motifs. Moreover, it can be photo-crosslinked quite quickly providing shape fidelity and stability at physiological temperature, but it has poor mechanical strength [46, 47]. Hence, the addition of PEGDA could improve the mechanical performance of the printed scaffolds maintaining simultaneously the possibilities for enhanced cell attachment, since PEGDA has tunable mechanical properties, but is not able to promote cell spreading and proliferation due to the absence of cell adhesion residues [48, 49].

Another major challenge that hinders the successful biofabrication of stable scaffolds with potential clinical applications is their limited mechanical properties [27]. Even though each printing technique utilizes a different working principle, the layer-by-layer method generally faces difficulties in the development of hollow structures. This happens since during a simple printing process with a single material, the introduction of a void in one layer can lead to possible collapse of the subsequent layer, which will be not properly connected to the previous one. This phenomenon affects negatively the structural integrity of the fabricated scaffolds, especially at the interfaces of droplets and lines in the cases of inkjet, LAB and extrusion based printing methods resulting in de-

formed geometries and offset features. This issue could be overcome to some extent with the use of sacrificial materials that could offer mechanical support to the subsequent layers during the printing process and would be removed after the attainment of the desired design. However, the incorporation of a sacrificial material increases the complexity of the printing procedure due to the requirement of multiple nozzles for dispensing different inks, the fast exchange of materials during the printing and the cyto-compatible removal of the sacrificial material after the scaffold formation [50–52]. These kind of complexities could be avoided with the use of lithography-based printing methods, which emerging as one of the most promising bioprinting methods for the development structurally integral scaffolds with complicated hollow features.

As it was previously described, 3D lithography has three different light patterning techniques, which have been used in several biomedical applications. Comparing the SLA and DLP printing, the DLP method holds the significant advantage of reducing considerably the printing time, which is extremely valuable for the fabrication of pre-seeded with cells scaffolds [24, 28, 29]. Among the three techniques, the 2PP one offers the best resolution allowing the creation of sub-micron feature sizes. However, these 2PP systems can typically create parts with dimensions smaller than 1 mm^3, which are not practical for the development of tissues usable for implantation and it has also low printing speed [30–32]. Consequently, DLP printing appears to be the most attractive technique for the fabrication of critical size, cell-friendly hydrogel-based scaffolds and it is the one that will be used in the present work.

1.4 Research questions

Inspired from the challenges encountered in the constantly developing hydrogel-based bioprinting field, the research questions emerging for the present work are the following:

- What kind of components need to be used for the development of an optimal bioresin, which will facilitate the handling, as well as the printing resolution of the DLP printing method?
- What kind of constructs can be printed with the selected printing method and the optimized bioresin?

- What is the mechanical performance of the printed scaffolds?

- What is the biological performance of the pre-seeded and post-seeded fabricated scaffolds in terms of cell-viability and proliferation?

1.5 Aim of study

In the present study, efforts are focused on the development of an optimal hydrogel-based bioink, which will be used for the DLP printing of cell-friendly and mechanically stable architectures for soft tissue engineering applications.

Different hydrogel combinations were tested and after the selection of the most optimal components, the characterization of the finally selected hydrogel bioresins was performed. Consequently, porous scaffolds were printed and mechanically tested, while cell viability and proliferation studies were performed for both bioprinted and post-seeded hydrogel scaffolds.

Chapter 2

Materials and Methods

2.1 Components of hydrogel bioinks

- GelMA synthseis

  For the synthesis of GelMA, gelatine (Sigma-Adrich, fish skin) was dissolved in PBS at a 10% w/v. concentration. 0.6g of methacrylic anhydride per gram of gelatine was added dropwise to the gelatine solution and left to react for 1h at 50 $^{\circ}C$ (**Figure 2.1**) under constant stirring. After the 1:1 dilution with pre-warmed (50 $^{\circ}C$) PBS0, the solution was transfered to 50 ml sterile falcon tubes, centrifugated at 4000 $rpms$ for 5 minutes so that any unreacted compound can sediment. Using a pipette-boy the solution was transferred to a container and titrated to 7.4 pH. Consequently, it was dialyzed in Milli Q water using a 12 kDa cutoff dialysis tubing for one week at 4 $^{\circ}C$, while the water was changed every day in order to remove any impurities, like unreacted MA and methacrylic acid byproducts, which can be cytotoxic. After the dialysis, the purified GelMA solution was sterile-filtered, freezed at -80 $^{\circ}C$ and then freeze-dried for 7 days in order to create the white porous foam, which was stored at 4 $^{\circ}C$ for further use. The degree of methacryloyl substitution was quantified to be 80%.

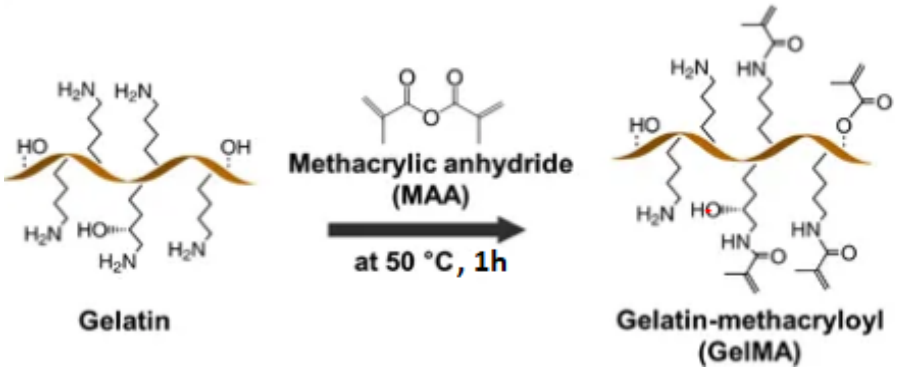

Figure 2.1: GelMA synthesis scheme.

- Poly(ethylene glycol) diacrylate (PEGDA, average Mn 700) was purchased from Sigma-Aldrich and the visible light sensitive photoinitiator Lithium phenyl-2,4,6-trimethylbenzoylphosphinate (LAP) from the Tokyo Chemical Industry CO.

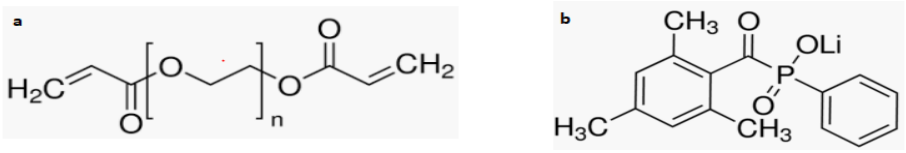

Figure 2.2: Structural formula of (a) PEGDA and (b) LAP.

- Yellow food dye was purchased from Queen Food Colour, Australia and used in the mixture of the hydrogel precursor solutions in order to work as a photoabsorber suitable for the reduction of the light penetration depth (Cd).

- Prior to the final choice of the aforementioned components for the development of an optimal bioink, a few more combinations were tested during the performance of preliminary experiments. These combinations included the blend of GelMA with LAP, as well as the mixture of GelMA with poly(ethylene oxide) (PEO) using an innovative visible light photoinitiating system from tris-bipyridyl-ruthenium hexahydrate (ru) and sodium persulfate compound (SPS). More information regarding these first exploratory experiments can be found in the Appendix A1.

2.2 Preparation of hydrogel bioinks

Freeze-dried cold fish GelMA with 80% of functionalization (DoF) was dissolved in PBS inside a 50 ml falcon tube until obtaining a stock solution of 20% (w/v). For the facilitation of dissolution, the tube was warmed on a roller plate located inside an incubator (at 37 $^{\circ}C$). PEGDA and LAP were also dissolved in PBS obtaining stock solutions of 40% and 2%, correspondingly. A vortex mixer was used to ensure the homogeneous blend of the solutions.

In order to find the final concentrations of the optimal hydrogel precursor solution, which could be used for DLP printing of mechanically stable and at the same time, cell-friendly hydrogel structures, different combinations of concentrations were tested. For all the combinations, the concentration of GelMA and LAP remained 10% and 0.2%, correspondingly. Three different concentrations of PEGDA, 5%, 10% and 15% were investigated, since it was hypothesized that the addition of this component could improve the mechanical properties of the resultant hydrogels, demonstrating proportionally increased compressive modulus with the concentration of PEGDA.

Finally, different concentrations of yellow dye were tested in an effort to control the printer's light penetration depth and render the printing process more tunable. This could be explained with the schematic diagram of **Figure 2.3**. As can be observed, the use of no/or a small quantity of photoabsorber allows the light to penetrate deeper into the photo-sensitive resin leading to overcuring and clogging of the channel. On the other hand, the use of excessive photoabsorber, leads to inadequate curing depth, which prevents the next printed layer to adhere or bond properly to the previous layer resulting in unstable prints prone to collapsing.

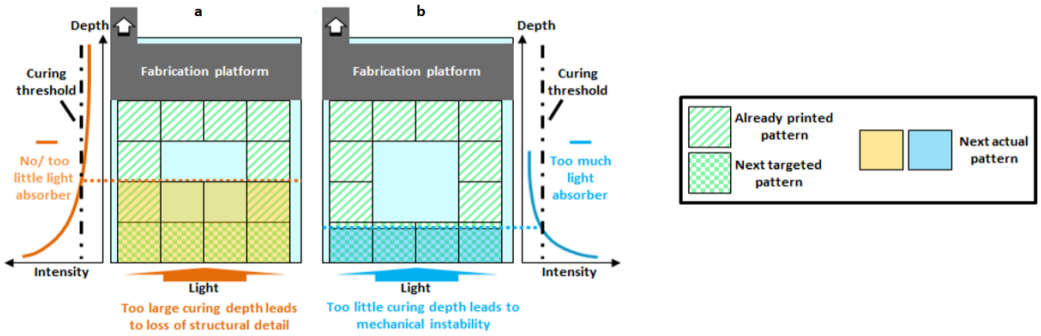

Figure 2.3: A schematic representation of the effects of curing depth on using DLP technology for printing hollow structures [56]. (a) Use of no or too little photoabsorber in resin formulation leads to overcuring and low resolution prints (e.x clogged channels). (b) Too much photoabsorber leads to undercuring and mechanically instable prints.

The tested hydrogel conditions were the following:

- 5% PEGDA + 10%GelMA + 0.2% LAP + 2% yellow dye
- 5% PEGDA + 10%GelMA + 0.2% LAP + 2.5% yellow dye
- 5% PEGDA + 10%GelMA + 0.2% LAP + 2.7% yellow dye
- 10% PEGDA + 10%GelMA + 0.2% LAP + 2% yellow dye
- 10% PEGDA + 10%GelMA + 0.2% LAP + 2.5% yellow dye
- 10% PEGDA + 10%GelMA + 0.2% LAP + 2.7% yellow dye
- 15% PEGDA + 10%GelMA + 0.2% LAP + 2.7% yellow dye
- 15% PEGDA + 10%GelMA + 0.2% LAP + 2.8% yellow dye

2.3 DLP printing system

Atum3D DLP Station V2.0 was the printer utilized for the experiments of the present thesis project. The printer has a light source of 405 nm, which is violet

light, classified in the visible range. **Figure 2.4** depicts some of the printer's characteristics.

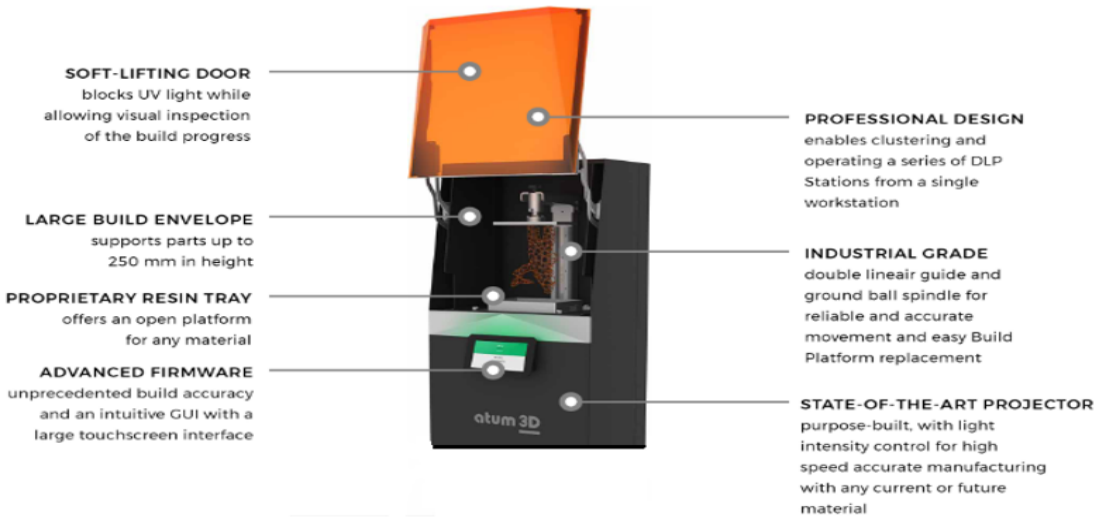

Figure 2.4: Characteristics of Atum3D DLP Station V2.0 [53].

2.4 Printing optimization of hydrogel bioinks

For the printing of complex structures with high fidelity via the DLP stereolithography method, the resin as well as, the printing parameters need to be optimized. In order to achieve that target, different combinations of the resin's components had to be tested, since differences in the resin's synthesis lead to differences in the absorption spectra and thus to the light penetration depths and cure depths.

When a laser beam is scanned over a layer of liquid photosensitive material, the irradiation penetrates the photopolymer and starts the curing. Based on the Beer-Lambert law of absorption, this light penetration is attenuated as result of either the distance through a chemical solution or the increase of the solution's concentration. According to this law, the light energy exposure $E(mJ/cm^2)$ declines with the depth z exponentially, following the equation 2.1 [54]:

$$E_z = E_0 e^{-z/D_p} \tag{2.1}$$

where E_z is the laser energy in the depth z, E_0 is the energy at the surface of the resin and D_p the light penetration depth of the resin at the specific wavelength.

The light penetration depth (D_p) along with the cure depth (C_d) and the critical energy exposure (E_c) are key parameters, which describe a photopolymer's behavior. The penetration depth is defined as the distance where the light is decreased to $1/e$ of its value on the resin surface. The cure depth is defined as the distance where the resin is solidified and critical energy is the threshold value at which, the resin transitions from the liquid to the solid phase (gelation point). The relation between these three parameters is described from the following equation 2.2 [55]:

$$C_d = D_p \ln(E_{max}/E_c) \tag{2.2}$$

where E_{max} is the laser energy at the resin surface.
The semi-log plot of cure depth upon the energy exposure results in a linear expression which is known as working curve. The slope of this curve is precisely the light penetration depth (Dp) at the laser wavelength used to generate the curve, while the x-axis intercept is the critical energy exposure of the resin (Ec) that indicates the gel point of the resin.

Based on the constructed working curves, the optimal printing parameters can be selected, taking under consideration a general rule of thumb, according to which the cure depth should be approximately double of the layer thickness (i.e step increment of the printer). This ensures that two subsequent layers will be attached to each other during the layer-by-layer printing of a structure.

For each of the tested hydrogel conditions, a working curve was created. In order to achieve that, the tested hydrogel precursor solutions were pipetted on a glass slide located at the basin of the printer and they were consequently exposed to different irradiation dosages for different time durations. To ensure that there was the same quantity of resin exposed to the laser beam, but also to avoid any chance of oxygen inhibition, a custom-made silicon mold was attached on the glass slide and 150 μl of resin were pipetted within its walls. Once the resin was exposed to different light intensities and time durations, gels with different thicknesses were created. The time exposure was varying from 2 to 4 sec, while the light intensity from 100%, 90% and 80%, where the 100% intensity corresponded to 15 mW/cm^2 according to the printer specifications.

Once the gels were created, distilled water was used to wash them from any residues of uncrosslinked material and consequently, the thickness of their crosslinked layers (cure depth, C_d) was measured using a stereo microscope. The

plot of cure depth against the corresponding irradiation energy, which was calculated from the multiplication of light intensity (mW/cm^2) with the corresponding time exposure (sec) (Energy=Light intensity x Exposure time), led to the formation of working curves, following the equation 2.2, as it has been previously described.

For each of the produced working curves, the critical energy (E_c), as well as the light penetration depth (D_p) were calculated.

Based on the working curves, the calculation of the aforementioned critical parameters and the rule of thumb, three different printing conditions were defined for three bioinks, each one corresponding to a different PEGDA concentration (5%, 10% and 15% PEGDA).

In order to optimize these bioinks in terms of their printing resolution and check the ability of the Atum3D printer to produce with them hollow structures with high fidelity, a cube 5 x 5 x 5 mm with 2 mm diameter channel had to be printed. To ensure the attachment of the print to the building plate, a 0.5 mm base was added to the original design (**Figure 3.4a**).

2.4.1 Investigation of spatial printing resolution

After the successful printing of the test cube with 2 mm diameter, the next step was the further assessment of the spatial printing resolution of the selected bioinks. To achieve this target, both positive and negative features were printed. Consequently, the designs with the printed dimensions of the features were measured and compared. The smaller were the differences, the better would be the printing resolution.

The positive test design (7 x 6 x 3 mm) had pillars with the same height (1 mm), but different width varying from 1000 μm to 750, 500, 250, 100 and 50 μm (**Figure 2.5a**).

The negative design (11 x 5 x 2 mm) was consisting of perfusable channels with different diameters ranging again from 1000 μm to 750, 500, 250, 100 and 50 μm (**Figure 2.5b**).

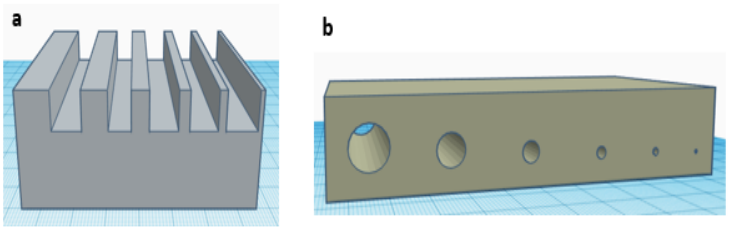

Figure 2.5: (a) CAD design of positive features. (b) CAD design of negative features.

2.5 Characterization of final optimal hydrogel bioinks

After the investigation of the bioinks, in terms of their spatial printing resolution, only the ones with 10% and 15% PEGDA were chosen as the most optimal ones, since the one with 5% PEGDA led to the creation of weak structures (See Results at section 3.1.4). The next step of the research included the characterization of these bioinks in terms of their crosslinking efficiency and mechanical properties (bulk material properties).

At this point it is important to mention the appearance of a complication during the conduction of the present study, which significantly affected the rest of the research work that was finally performed. Particularly, the experiments for the optimization of the printing resolution were completed by the mid of July 2019 and several preliminary scaffold designs were printed by the mid of August. The continuity of the research work started again towards the end of September, however, after that time point, the optimized bioinks stopped to produce the previously well-defined prints. To be more specific, all the efforts to print the previously fabricated preliminary designs with the originally optimized bioinks and printing parameters, were leading to the creation of unfinished prints that were detached from the building plate during the printing process. All the trials to resolve this problem in order to print again complete, mechanically stable scaffolds with high resolution, are thoroughly described in the section 4.3.1 (Problems with Atum3D printer), as well as, the Appendix A3 (Trials to fix the problem with Atum3D printer). From all the trials that were totally performed, a few scaffolds made from the bioink with 10% PEGDA and 15% PEGDA, correspondingly, were printed with decent printing resolution. However,

both the bioinks' synthesis and the printing parameters had to be re-defined.

Consequently, the characterization of the bioinks was performed for the re-optimized bioinks.

2.5.1 Crosslinking efficiency

Six cylindrical, non-porous samples with $4mm$ diameter and $1mm$ height were printed with the Atum3D printer for each of the final re-optimized bioinks. Mass loss and swelling studies were performed based on previously published protocols [57, 58].

Particularly, directly after printing the samples were weighed in order to measure their initial wet mass ($m_{initial}$). Consequently, they were frozen at $-80°C$ and then placed in the freeze dryer overnight. The next day, the samples were removed from the freeze-dryer and weighted again (m_{dry1}). The actual macromer concentration was calculated from the following equation (2.3):

$$\%macromer = \frac{m_{dry1}}{m_{initial}} * 100\% \tag{2.3}$$

The same samples were submerged in excess volume of PBS and left overnight to the incubator at $37°C$ to rehydrate. The following day, the samples were weighed $m_{swollen}$ and then freeze-dried overnight for the second time. The next day, they were weighted again (m_{dry2}). The swelling ratio (q) was calculated from the equation (2.4), while the sol fraction from the equation (2.5):

$$q = \frac{m_{swollen}}{m_{dry2}} \tag{2.4}$$

$$\%mass\ loss = \frac{m_{dry1} - m_{dry2}}{m_{dry1}} * 100\% \tag{2.5}$$

The sol fraction constitutes a measurement of the uncrosslinked macromers in the hydrogel network and can be basically found from the mass loss at day 1 [57] .

2.5.2 Mechanical properties of bulk materials

Discs with $6mm$ diameter and $2mm$ height were printed with the Atum3D printer using the aforementioned re-optimized bioinks in order to evaluate their mechanical properties. Four samples for each of the two bioinks were created

and consequently, subjected to unconfined stress-relaxation tests with a Dynamic Mechanical Analyzer (Q800 DMA, TA Instruments, USA). Five different strain rates, varying from $15\%/min, 25\%/min, 30\%/min, 300\%/min$ and $500\%/min$ were investigated, while the strain ramp was set up to -15% strain for 5 min, for all the different strain rates. For each of the different strain rates, four repeats of the same test were performed. The initial displacement was set at $0\mu m$, but a small preload force of 0.001 N was applied in order to ensure the attachment of the compression clamp to the tested samples. Finally, the data sampling interval was set as 0.10 s/pt to achieve the measurement of 10 points per sec. The corresponding stress-time curves were plotted, while the maximum and equilibrium stress, as well as, the percentage of relaxation and the equilibrium modulus were defined for each of the different strain rates and compared between the samples made from bioinks with 10% and 15% of PEGDA.

2.6 Design of porous scaffold

In order to exploit the advantage of the DLP printing technology to fabricate hollow structures with high resolution and structural integrity, a porous scaffold was designed using the TinkerCAD (Autodesk, USA) software. It was hypothesized that the combination of a porous macrostructure along with the hydrogel bioink could improve significantly the oxygen and nutrients' diffusion in the scaffold's interior, overcoming one of the major limitations of current scaffolding techniques. The CAD design of the printed porous scaffold can be seen in Figure 2.6. The initial geometry of the building cell, which was used for the creation of the complex cubic architecture, was quite simple. Particularly, a hollow sphere with 1.7 mm diameter was placed centrally into a solid cube 1.5 x 1.5 x 1.5 mm and merged. The result of the cube with a cavity inside constituted the building cell. By replicating 6 of these cells along the three normal directions and consequently, cutting in half both of the end cells in all directions, the design illustrated in **Figure 2.6** was created. The final cubic scaffold had 7.5 mm facets and pores with 700 μm diameter. A base of 0.5 mm height was added to the final CAD design in order to ensure the attachment of the cubic scaffold to the building plate during the fabrication process.

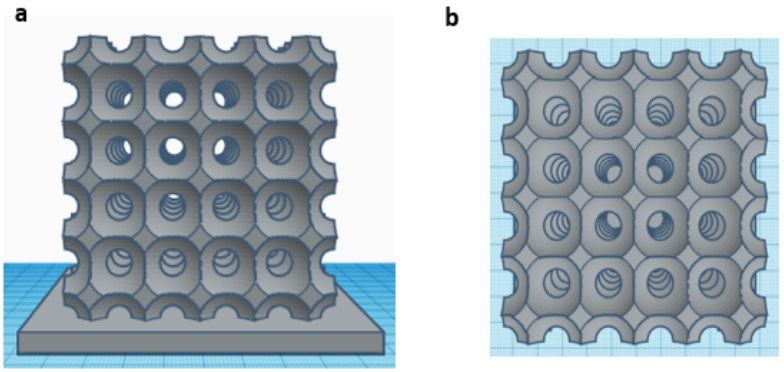

Figure 2.6: CAD design of scaffold. (a) Side view and (b) top view.

2.7 Mechanical characterization of porous scaffolds

Four scaffolds made from each of the two re-optimized bionks ($n = 4$) were utilized for the characterization of their mechanical response under the performance of unconfined stress-relaxation tests. The same tests and conditions used for the mechanical characterization of the solid discs were also applied for the scaffolds. (See section 2.5.2 Mechanical properties of bulk materials).

2.8 Cell culture

Mesenchymal stem cells (MSCs) were used for the bioprinting and post-seeding of hydrogel scaffolds. MSCs were cultured in Dubeco's Modified Eagle Medium (DMEM, Thermo Fisher Scientific, USA) supplemented with 10% Fetal bovine serum (FBS), 1% Penicillin/streptomycin (P/S) and 1 $\mu l/ml$ basic fibroblast growth factor (bFGF, R&D Systems). The cells were cultured up to passage 3 before the experiments' performance.

2.9 Bioprinting and post-cell seeding of hydrogel scaffolds

For the experiments where the cells had to be encapsulated and seeded on the hydrogel scaffolds, only 2 out of the 7.5 mm height scaffold were printed in order to perform the cell viability and proliferation tests, as a proof of concept.

For this purpose, the two re-optimized bioinks were prepared and sterilized with 0.22 μm filters at the flow cabinet. The final concentration of cells used for encapsulation was $5 * 10^6 cells/ml$, while for seeding 10.000 $cells/cm^2$.

The baseplate and building plate were kept in ethanol for 30 min in order to make them sterile, while the printer was thoroughly cleaned with ethanol. Before starting the printing procedure, the ethanol was removed from the baseplate, as well as, the building plate and they were let to air dry. The tested hydrogel (re-optimized) bioinks were taken from the flow cabinet and added to the printer using a pipette with sterile tips. When a print was finished, it was transferred to a sterile 6-well plate with the use of an autoclaved spatula. Consequently, it was taken to the flow cabinet, transfered again to a new sterile 48-well plate to eliminate any contamination possibility and washed with sterile PBS0 for $10min$. For the bioprinted samples, fresh culture medium was added in the corresponding wells and the plate was placed in the incubator at 37°C. For the scaffolds that had to be seeded, 10 $\mu g/ml$ fibronectin was used as coating in order to promote cell adhesion, since fibronectin is a high molecular weight protein of the extracellular matrix (ECM), which plays significant role in cell adhesion, growth, differentiation and migration [61, 62]. After 1 h of incubation at 37°C, the samples were washed 3 times with PBS0 and finally seeded with cells. All the scaffolds were cultured for 10 days, while the medium was changed every 2-3 days.

2.10 Cell viability and proliferation tests

2.10.1 Live/Dead Assay

The cell viability of hydrogel scaffolds with both encapsulated and seeded cells was tested performing a live-dead assay, at day 2 and 7 of culture. 0,25 μl calcein AM and 0,5 μl ethidium homodimer per ml of PBS were used for the assay and four different samples were tested ($n = 4$). Images were taken using fluorescence microscope, which was showing living cells in green (where the calcein AM binds, with a 488/530 nm excitation/emission filter) and dead cells in red (where the ethidium homodimer binds, with a 530/580 nm excitation/emission filter). Live and dead pictures of 3 sections per sample were taken, at 10x magnification of the microscope. The living and dead cells were counted with the ImageJ software. The cell count from all sections of the same hydrogel was summed, and the viability ratio was obtained from the equation:

$$Cell\ viability = \frac{living\ cells}{dead\ cells} * 100\% \tag{2.6}$$

2.10.2 Alamar Blue Cell viability assay

The Alamar Blue assay is used to quantitatively measure the proliferation of cells. It utilizes an active ingredient named resazurin, which is a non-toxic, cell-permeable compound with blue color and virtually non-fluorescent ability. Upon entering living cells, resazurin is reduced to resorufin which is a red and highly fluorescent compound. This means that increased cell viability and proliferation is observed when the color becomes more red. These changes in viability can be easily detected using an fluorescence-based plate reader. 300 μl of 10% Alamar Blue (dye) in culture medium were used to cover completely the tested samples ($n = 4$), and after 4 hours of incubation, the change in color was detected. The assay was performed for day 1, 4, 7 and 10 of culture, in order to observe the proliferation of cells over a period of 10 days.

2.11 Statistical analysis

The statistical analysis of the results was performed using the GraphPad Prism 8 software package. All the data are represented as average and standard deviation of independent replicates (n=4-6). A t-test and two-way ANOVA tests, with subsequent Bonferroni tests, were performed to find significant statistical differences between conditions. Different degrees of significance were taken into account: * for $p < 0,05$, ** for $p < 0,01$, *** for $p < 0,001$ and **** for $p < 0,0001$.

Chapter 3

Results

3.1 Printing optimization of hydrogel bioinks

3.1.1 Development of working curves

The working curves produced for each of the tested hydrogel bioinks were assorted into three graphs based on the concentration of PEGDA that was included in their synthesis. **Figures 3.1** to **3.3** illustrate the working curves for the bioinks with 5%, 10% and 15% PEGDA, accordingly. For the creation of the curves, the measured thickness of the produced gels, which corresponds to the cure depth C_d, was plotted against the corresponding energy exposure. For each printing condition (set of energy and time exposure), the thickness of four different gels (n=4) was measured. (Tables with all the printing conditions, as well as, the measurement results are presented in the Appendix A2.

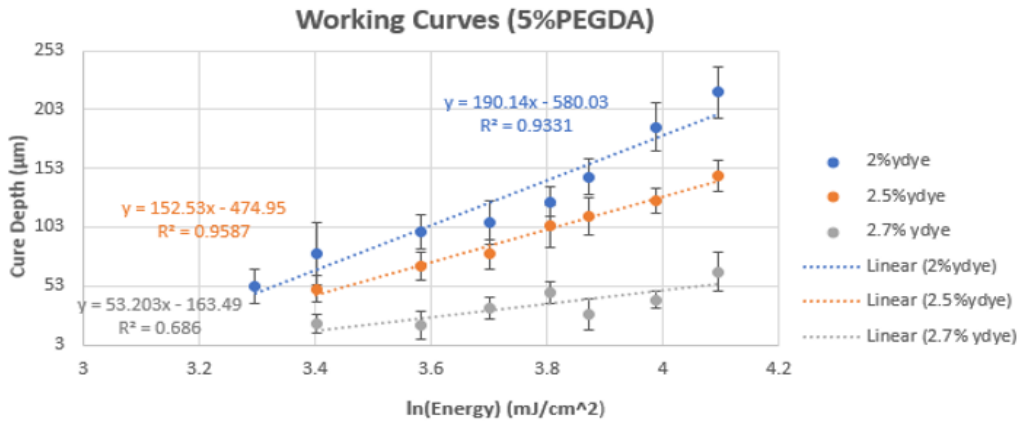

Figure 3.1: Working curves for the tested bioinks with 5% PEGDA and three different concentrations of yellow dye: 2%, 2.5% and 2.7%.

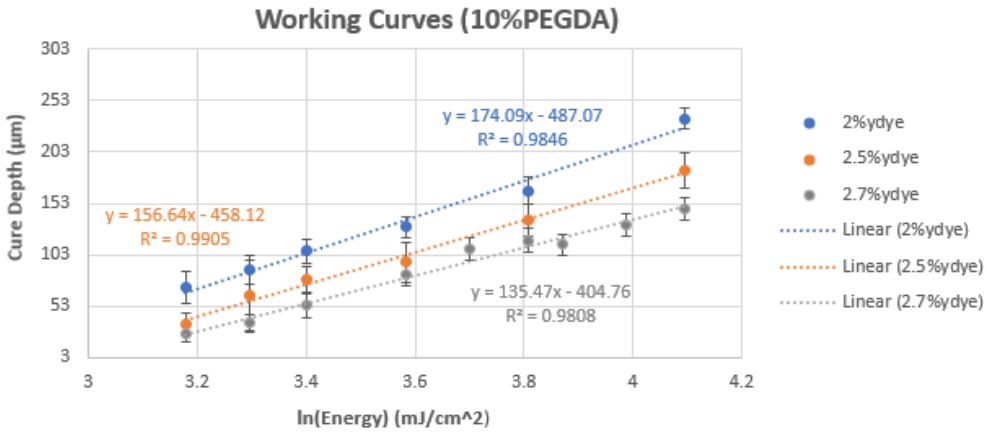

Figure 3.2: Working curves for the tested bioinks with 10% PEGDA and three different concentrations of yellow dye: 2%, 2.5% and 2.7%.

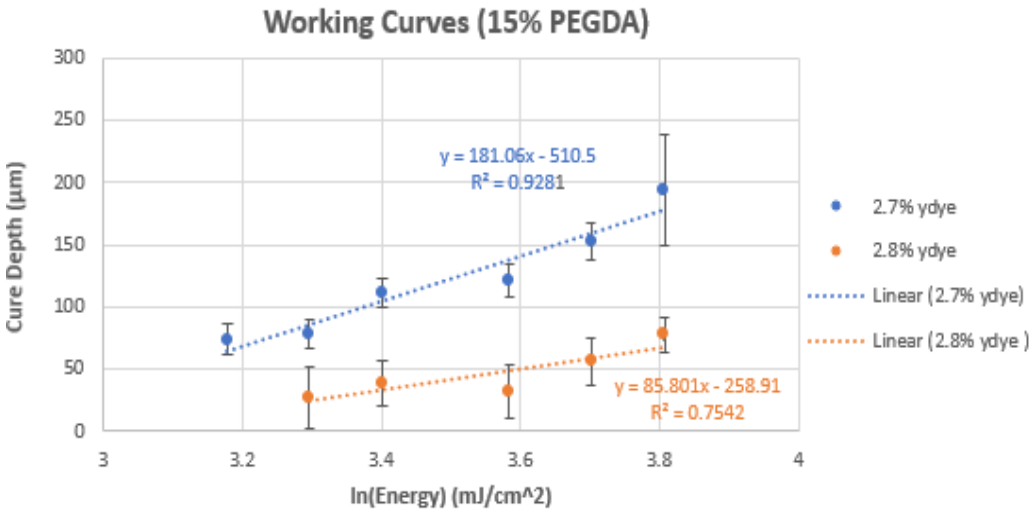

Figure 3.3: Working curves for the tested bioinks with 15% PEGDA and two different concentrations of yellow dye: 2.7% and 2.8%

3.1.2 Calculation of the critical energy and light penetration depth

For each of the working curves, the trendlines along with their equations are also depicted in **Figures 3.1**, **3.2** and **3.3**. These equations were utilized for the calculation of the light penetration depth (D_p) and the critical energy (E_c), as can be seen in Table 3.1, following the equation (2.2):

$$C_d = D_p \ln(E/E_c) \Rightarrow C_d = D_p \ln E - D_p \ln E_c \tag{3.1}$$

where in the case of a trendline in the form $y = ax - b$, $y = C_d$, $x = \ln E$, $a(slope) = D_p$, while the E_c is calculated as follows:

$$b = D_p \ln E_c \Rightarrow E_c = e^{b/D_p} \tag{3.2}$$

Condition		Ec (mJ/cm^2)	Dp (μm)
5% PEGDA	2% dye	21.13	190.14
	2.5% dye	22.5	152.53
	2.7% dye	21.6	53.203
10% PEGDA	2% dye	16.4	174.09
	2.5% dye	18.63	156.64
	2.7% dye	19.84	135.47
15 % PEGDA	2.7% dye	16.77	181.06
	2.8% dye	20.44	85.81

Table 3.1: Values of the critical energy (E_c) and the light penetration depth (D_p) for each of the tested bioinks.

3.1.3 Test cube design print

After the assessment of the working curves along with the critical energy and the light penetration depth for the tested hydrogel conditions, the definition of the optimal bioink synthesis and their printing parameters was attempted. This effort started with the bioinks having 10% PEGDA since it is the intermediate concentration.

For the 10% PEGDA working curve and after calculating the critical energy (E_c) for each of the three different examined conditions, it can be observed that the increase of yellow dye led to an increment of the critical energy from 16.408 mJ/cm^2 to 18.63 mJ/cm^2 and 19.84 mJ/cm^2 for 2%, 2.5% and 2.7% of dye, correspondingly. This resulted in the reduction of the light penetration depth (D_p), which is extremely valuable in the DLP printing technology since it offers the opportunity for fabrication of structures with higher resolution. Hence, 2.7% yellow dye was utilized in the bioink with 10% PEGDA, 10%GelMA and 0.2%LAP. Since low printing time, as well as, increased resolution are requirements for printing structures with high fidelity as fast as possible, the printer parameters were set at 100% light intensity exposure (15 mW/cm^2), 2 sec time exposure (lowest tested time), while the layer thickness was set at 25 μm based on th rule of thumb, as it has been earlier mentioned (layer thickness should be approximately half of cure depth). (These values were selected as prospective optimal printing parameters based on the working curve for 10% PEGDA and 2.7% dye - See Table Appendix A2). With these conditions, the 5 x 5 x 5 mm

cube with a channel of 2 mm diameter was about half way printed, as can be seen in **Figure 3.4b**. This result indicated that the previous settings did not allow sufficient crosslinking. In order to solve this issue, the time exposure was increased from 2 to 3 sec leading eventually to the print of a cube with a channel almost completely blocked due to over-curing (result not shown). In order to reduce the crosslinking efficiency and achieve the opening of the channel, the light intensity was reduced to 80%, (12 mW/cm^2) and the layer thickness was set at 40 μm based on the corresponding working curve and the general rule of thumb. Particularly, since the cure depth for the specific condition was measured at around 83.19 μm (Table Appendix A2), the layer thickness should be set a bit smaller (or approximately half) to ensure a sufficient bonding between neighboring layers. With these conditions, the cube was printed, but the channel was not entirely open again (**Figure 3.4c**). To avoid the clogging, several trials were performed using the exact previous conditions, but increasing the layer thickness to 60, 70 and finally 80 μm, until an almost precise print of the cube CAD design was fabricated (**Figure 3.4d**). Consequently, the printing settings of 80% light intensity, 3 sec of time exposure and 80 μm layer thickness were used for printing structures with the bioink consisting from 10% PEGDA, 10%GelMA, 0.2% LAP and 2.7% yellow food dye.

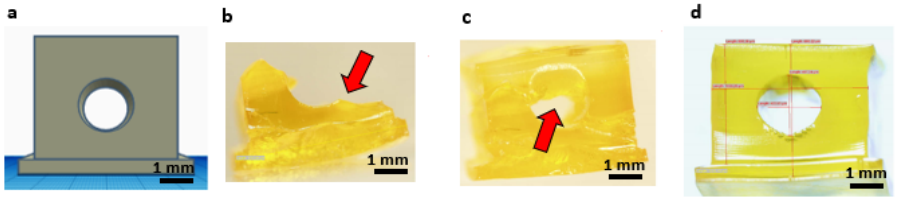

Figure 3.4: (a) CAD design of 5 x 5 mm cube with 2 mm diameter. (b) Unsuccessful print of cube using bioink from 10% PEGDA, 10% GelMA, 0.2% LAP and 2.7% yellow dye and setting as printing parameters 100% light intensity exposure, 2 sec time exposure and 25 μm layer thickness. (c) Print of cube with clogged channel using the same bioink as in figure (b) and setting as printing parameters 80% light intensity exposure, 3 sec time exposure and 40 μm. (d) Successful print of cube using the same bioink and printing parameters as in figure (c), except from the layer thickness, which was set at 80 μm.

In order to define the printing settings for the bioink with 15 %PEGDA, the corresponding working curves had to be studied. The increase in PEGDA concentration, led to increased crossilinking density, as can be observed from

the working curves (**Figures 3.2** and **3.3**). Particularly, the cure depths (C_p) for the gels created with 10% PEGDA were lower compared to the corresponding ones created with 15% PEGDA, for the same photoabsorber concentration (2.7% yellow dye).

The working curve plotted for the bioink with 15% PEGDA and 2.8% yellow dye resulted in a significantly reduced light penetration depth compared to 2.7% dye (see Table 3.1). This result demonstrated how decisive is the role of the photoabsorber concentration in terms of tuning the printing process through the reduction of the light penetration depth.

Since 80% light intensity, 3 sec time exposure and 80 μm layer thickness were set for the bioink with 10% PEGDA, the same conditions except from the time exposure were used for 15% PEGDA. It was hypothesized that the time exposure should be reduced from 3 to 2 sec due to the higher crosslinking density of the bioink with 15%PEGDA. The hypothesis was proven totally correct since it allowed the print of the cube with an open channel of 2 mm diameter.

For the bioink with 5% PEGDA, the same concentrations of photoabsorber as in the case of the bioink with 10% PEGDA were used. It can be again observed that the reduction of PEGDA concentration influenced significantly the crosslinking density of the hydrogels since the cure depths of the gels with 5% PEGDA were significantly lower compared to 10% PEGDA corresponding ones (see **Figures 3.1** and **3.2**).

Moreover, the measurements of cure depth for 5% PEGDA and 2.7% dye demonstrated a noticeable deviation from the trendline (coefficient of determination $R^2 = 0.686$) since the height of the created discs (cure depth) was quite small and difficult to be measured precisely at the optical microscope. Hence, the setting of the printing parameters was based on the bioink with 2.5% dye, which would potentially offer better resolution compared to 2% dye.

Following the opposite hypothesis as mentioned earlier with the working curve for 15% PEGDA, the same printing conditions defined for 10% PEGDA were used also for 5% PEGDA with the exception of time exposure. In this case the time was increased from 3 to 4 sec, since the reduction of PEGDA concentration from 10% to 5%, decreased the crosslinking efficiency of the bioink. The hypothesis was proven correct and the test cube design was printed successfully.

Consequently, the optimal bioinks, as well as, the required printing parameters for the DLP printing of hollow structures (with 2 mm diameter) were the following:

- Bioink 1: 5% PEGDA, 10% GelMA, 0.2% LAP and 2.5% yellow dye
  Printing parameters: 80% light intensity, 4 sec time exposure, 80 μm layer thickness
- Bioink 2: 10% PEGDA, 10% GelMA, 0.2% LAP and 2.7% yellow dye
  Printing parameters: 80% light intensity, 3 sec time exposure, 80 μm layer thickness
- Bioink 3: 15% PEGDA, 10% GelMA, 0.2% LAP and 2.7% yellow dye
  Printing parameters: 80% light intensity, 2 sec time exposure, 80 μm layer thickness

3.1.4 Investigation of spatial printing resolution

After the printing of the designs with positive and negative features, the dimensions of the features were measured with optical microscope and compared with the designed ones. These results are presented in the following tables.

Positive features			
Designed dimensions (μm)	Printed dimensions (μm)		
	5% PEGDA+2.5% dye	10% PEGDA+2.7% dye	15% PEGDA+2.7% dye
1000	1030 (?)	881.4512	852.6548
750	-	755.5285	603.7845
500	-	503.6869	487.5412
250	-	264.435	185.4785
100	-	125.9214	121.4781
50	-	-	57.4781 (?)

Table 3.2: Comparison between the designed and printed dimensions of the positive features for each of the three bioinks.

Negative features						
Designed dimensions (μm)	Printed dimenions (μm)					
	5% PEGDA+2.5% dye		10% PEGDA+2.7% dye		15% PEGDA+2.7% dye	
	x-direction	*y-direction*	*x-direction*	*y-direction*	*x-direction*	*y-direction*
1000	1098.853	979.6722	985.4781	932.4512	1133.0138	1053.459
750	892.815	793.6138	766.249	754.1248	803.7018	788.2365
500	549.425	482.3652	-	-	459.2365	421.8561
250	-	-	-	-	287.03	211.6587
100	-	-	-	-	114.81	97.2658
50	-	-	-	-	-	-

Table 3.3: Comparison between the designed and printed dimensions of the negative features for each of the three bioinks.

As can be observed from **Figure 3.5a**, positive features with dimensions smaller than 1000 μm could not be measured for the print with 5% PEGDA, since the pillars collapsed due to the soft nature of the hydrogel. (The pillars were able to retain their original position only under water immersion). The dimensions of positive features made from 10% PEGDA bioink appeared to be quite close to the designed ones, except from the first pillar which was measured a bit shorter (881,4512 μm). The pillar with 50 μm width collapsed, while in the case of 15% PEGDA, it was printed, but with the pass of time, it started to bend. For this reason, the symbol (?) was placed next to the value of his measured width. As far as the negative features, in the case of the print with 5% PEGDA, channels with diameter from 1000 to almost 500 μm were created. However, only the channels with 1000 and 750 μm diameter were perfused with a red food dye. For the 10% PEGDA print, channels with diameter only up to almost 750 μm were printed and able to be perfused, while the bioink with 15% PEGDA demonstrated the highest resolution allowing the print of negative features up to almost 100 μm. However, after testing the ability to perfuse the channels, only the ones with diameter up to 500 μm were perfusable.

Based on the aforementioned results, only the bioinks with 10% and 15% PEGDA were further investigated, since the 5% PEGDA bioink led to the creation of softer constructs.

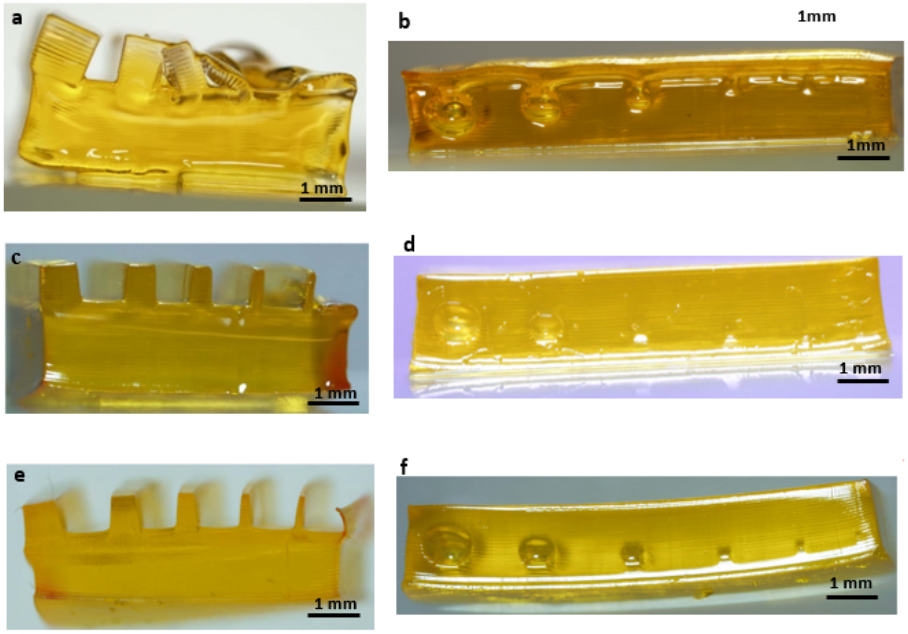

Figure 3.5: (a), (b) Positive and negative features printed with the Bioink 1: 5% PEGDA, 10% GelMA, 0.2% LAP and 2.5% yellow dye. (c), (d) Positive and negative features printed with the Bioink 2: 10% PEGDA, 10% GelMA, 0.2% LAP and 2.7% yellow dye. (e), (f) Positive and negative features printed with the Bioink 3: 15% PEGDA, 10% GelMA, 0.2% LAP and 2.7% yellow dye. In all the cases, the corresponding printing parameters for each bioink were utilized.

3.2 Characterization of optimal bioinks

The characterization of the bioinks in terms of their crosslinking efficiency and mechanical properties was not performed on the originally decided bioinks due the technical problems that appeared with the Atum3D printer, as it has been earlier mentioned and thoroughly explained in the section 4.3.1 and the Appendix A3. For this reason, the characterization was performed on the re-optimized bioinks that allowed the print of porous mechanically stable scaffolds with two different bioinks. The main difference of the re-optimized and the originally selected bioinks was related with the concentration of the photoabsorber

(yellow dye). Particularly, since the prints were continuously detaching from the building plate during the fabrication process, the dye concentration was significantly reduced in order to increase the light penetration depth and amplify the crosslinking efficiency. Particularly, the dye was decreased from 2.7% to 1.2% for the bioink consisting of 10%PEGDA, 10% GelMA and 0.2% LAP, and also from 2.7% to 1.4% for the bioink consisting of 15% PEGDA, 10% GelMA and 0.2% LAP.

3.2.1 Crosslinking efficiency

The characterization of the re-optimized bioinks in terms of their crosslinking efficiency led to the creation of the graphs illustrated in **Figure 3.6**. As far as the macromer concentration, the 15% PEGDA bioink seemed to have higher percentage ($\simeq 23.83\%$) compared to the 10% one ($\simeq 20.08\%$). On the contrary, the swelling ratio (q) for the 10% PEGDA bioink ($\simeq 5.8\%$) was higher from that of 15% PEGDA ($\simeq 4.7\%$), as it was expected, due to the lower crosslinking density of the bioinks with decreased PEGDA concentration. In terms of the sol fraction, the 10% PEGDA bioink demonstrated a smaller percentage ($\simeq 8.4\%$) compared to the 15% ($\simeq 9.5\%$) with no significant difference (p=0.5140).

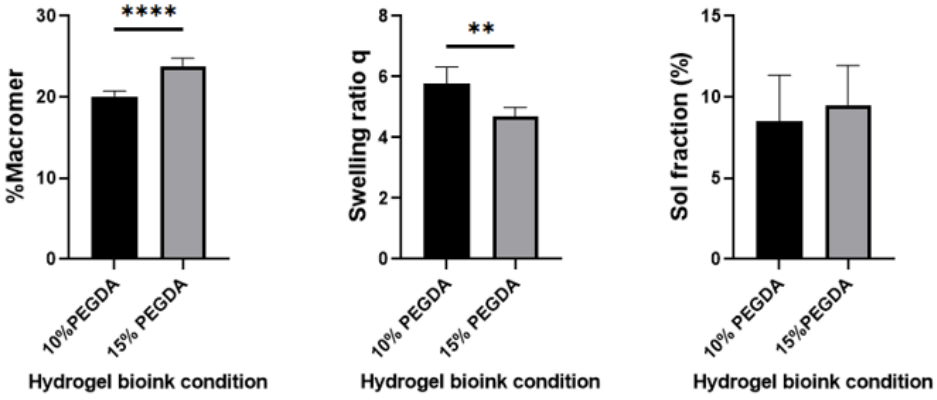

Figure 3.6: Results from the crosslinking efficiency characterization of the two re-optimized bioinks (consisting of 10% and 15% PEGDA). The percentage of macromer concentration (a), the mass swelling ratio q (b) and the percentage of sol fraction (c) are presented for each of the two bioink conditions. The data are expressed as mean $\pm$ standard deviation ($n = 6, *forp < 0.05, **forp < 0.01, ***forp < 0.001 and ****forp < 0.0001$).

3.2.2 Mechanical behavior of bulk materials

During the performance of stress-relaxation tests, a decrease in the stress is observed in response to the strain, which is held constant upon the structure. The stress-time curves of all the discs made from 10% and 15% PEGDA can be observed at **Figures 3.7 and 3.8**, respectively.

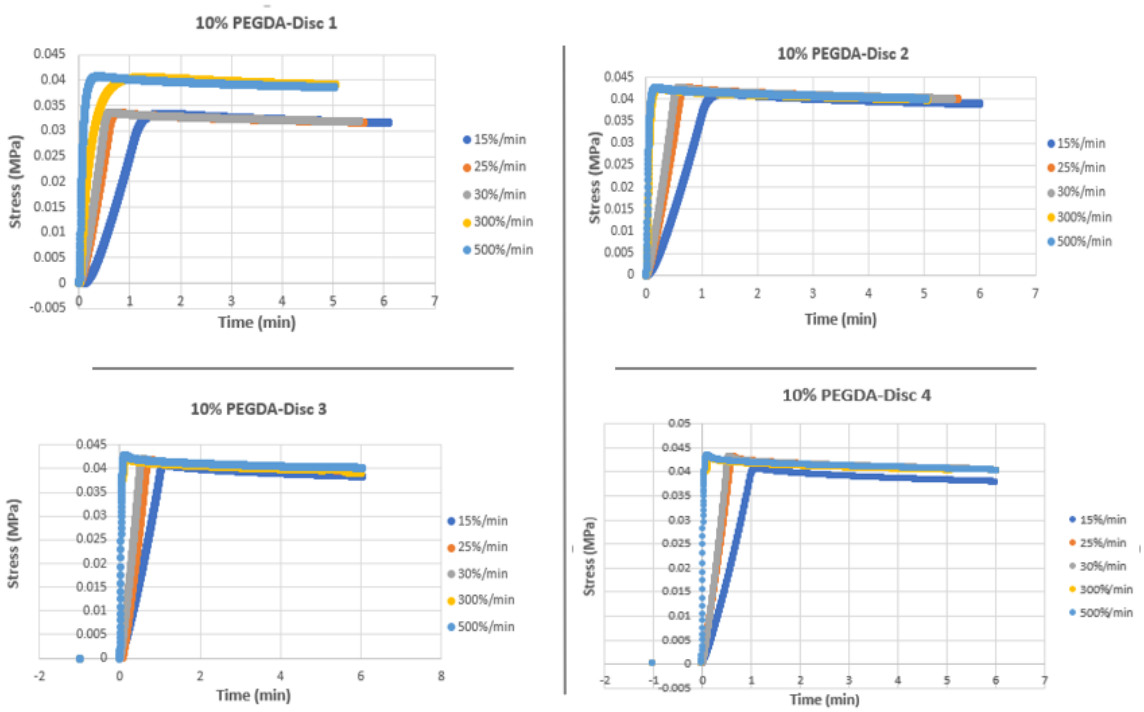

Figure 3.7: Stress-time curves of discs made from bioink with 10% PEGDA, after the performance of stress relaxation tests for five different strain rates ($15\%/min, 25\%/min, 30\%/min, 300\%/min$ and $500\%/min$) using a ramp strain -15%. Four discs with 10% PEGDA were tested (n=4).

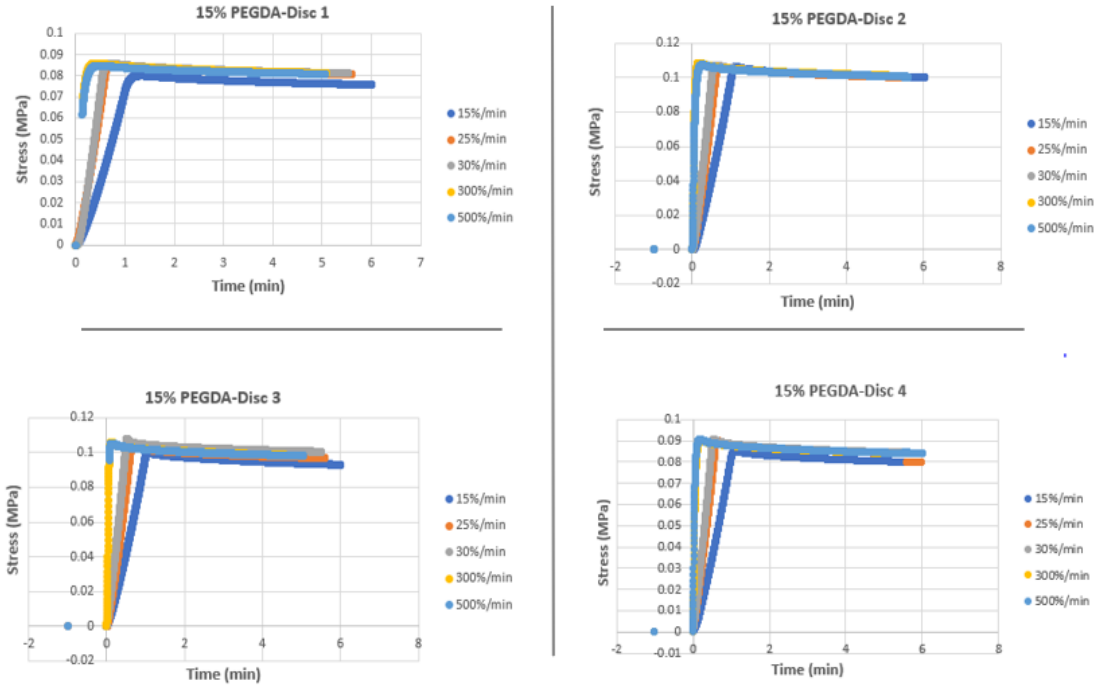

Figure 3.8: Stress-Time curves of discs made from bioink with 15% PEGDA, after the performance of stress relaxation tests for five different strain rates ($15\%/min, 25\%/min, 30\%/min, 300\%/min$ and $500\%/min$) using a ramp strain -15%. Four discs with 15% PEGDA were tested (n=4).

Figure 3.9 demonstrates the results from the mechanical characterization of the printed discs, which were subjected to stress-relaxation tests with five different strain rates. As can be observed, both the maximum and equilibrium stress were significantly higher for the discs made from the bioink with 15% PEGDA concentration since the increase of PEGDA led to the printing of stiffer hydrogel discs. For the same reason the equilibrium modulus was also much higher for the discs with 15% PEGDA. However, comparing the values of maximum and equilibrium stress, as well as the equilibrium modulus for the discs, which were printed with the same bioink, but subjected to different strain rates, only small differences can be detected between the strain rates. Particularly, the max stress for the discs with 10% PEGDA showed a small increase from 0.039 MPa to 0.042 MPa, as the strain rate increases from $15\%/min$ to $500\%/min$. For the discs made with 15%, PEGDA, the max stress increased slightly from 0.093 MPa to

approximately 0.098 MPa for the strain rates between $15\%/min$ and $300\%/min$, while showing a minor decrease to 0.096 MPa for the $500\%/min$ strain rate. The stress equilibrium for the discs with 10% PEGDA increased slightly and steadily from 0.037 to 0.039 MPa from the $15\%/min$ to the $500\%/min$ strain rate, and the same pattern appears for the 15% PEGDA discs with the corresponding values ranging from 0.087 to 0.090 MPa. As far as the equilibrium modulus is concerned, a small increase was also demonstrated with the values ranging from 0.24 to 0.26 MPa and from 0.58 to 0.60 MPa for the discs with 10% and 15% PEGDA, correspondingly. In terms of the relaxation percentage, a small decrease was observed for the 15% PEGDA discs compared to the 10% for all the tested strain rates, but no specific pattern can be detected comparing the different strain rates for the discs printed with the same PEGDA concentration.

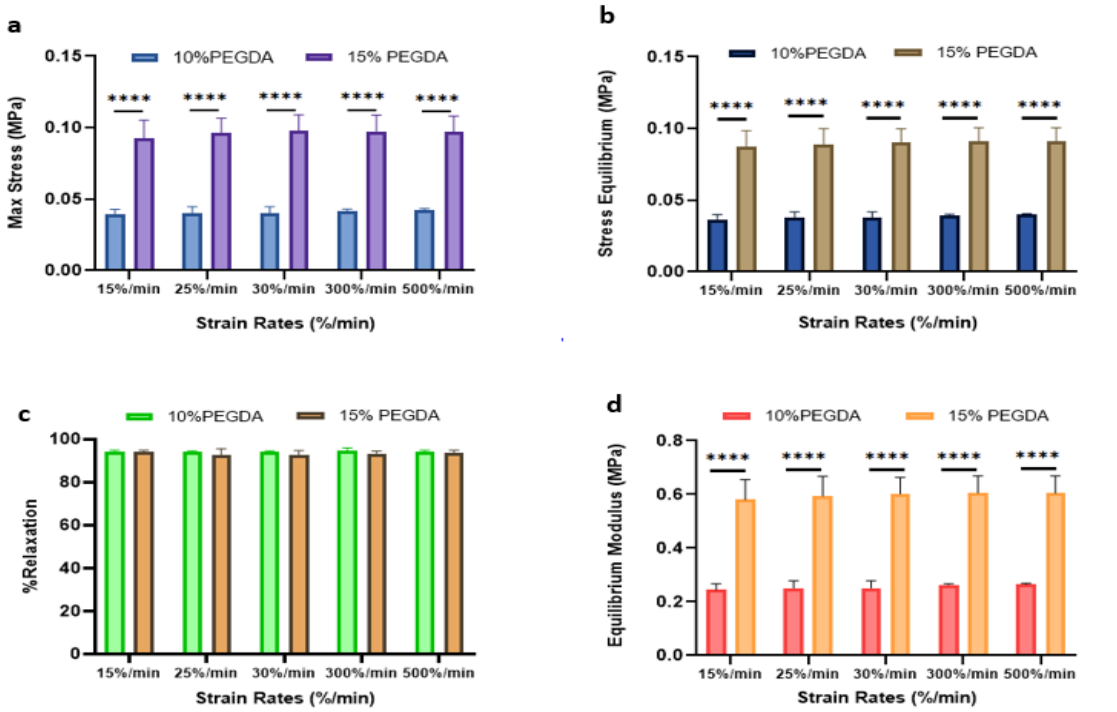

Figure 3.9: Results from the mechanical characterization of discs (bulk material properties of final optimal bioinks consisting of 10% and 15% PEGDA). The maximum (a) and equilibrium (b) stress, as well as, the percentage of relaxation (c) and the equilibrium modulus (d) are presented for each of the five different strain rates and directly compared between the two bioinks. The data are expressed as mean $\pm$ standard deviation ($n = 4$, * for $p < 0,05$, ** for $p < 0,01$, *** for $p < 0,001$ and **** for $p < 0,0001$).

3.3 Successful printing of hydrogel scaffolds

Due to the technical problems that appeared with the Atum3D printer, as it has been earlier described, the bioinks selected after the assessment of the working curves had to be re-optimized. During this procedure and after performing numerous trials to resolve the problem, a few decent prints of the porous design were fabricated. **Figure 3.10** depicts one of the successful prints of the scaffold using the re-optimized bioink consisting of 15% PEGDA, 10% GelMA, 0.2% LAP and 1.4% yellow dye.

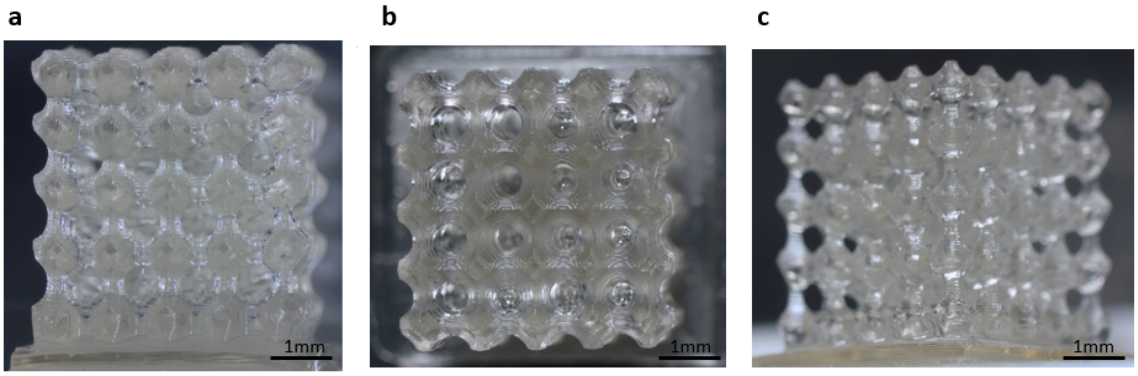

Figure 3.10: Print of porous scaffold with the re-optimized bioink consisting of 15% PEGDA, 10% GelMA, 0.2% LAP and 1.4% yellow dye. (a) Side, (b) Top and (c) Isometric view of the scaffold.

3.4 Mechanical characterization of hydrogel scaffolds

The stress-time curves of all the scaffolds made from 10% and 15% PEGDA are demonstrated in **Figures 3.11** and **3.12**, accordingly. After comparing the curves, it can be observed that the relaxation response is more prominent in the case of scaffolds compared to the discs, where the bulk material properties were investigated. Moreover, the noticeable deviations of the curves for the scaffolds made from 15% PEGDA, indicate possible structural differences between the samples.

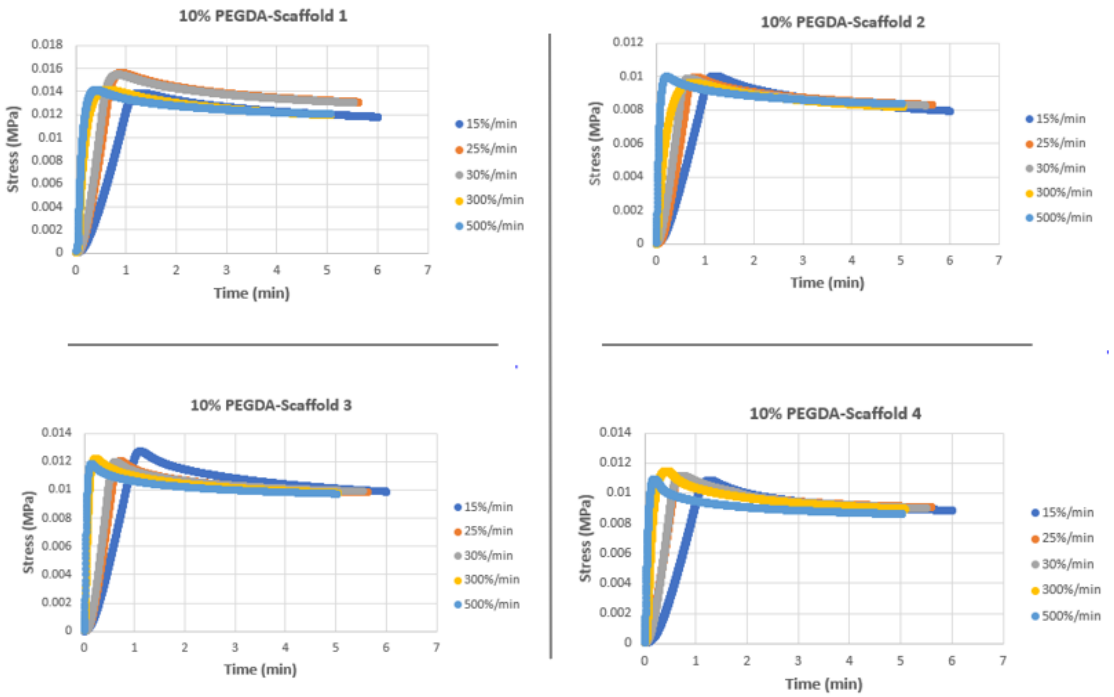

Figure 3.11: Stress-Time curves of scaffolds made from bioink with 10% PEGDA, after the performance of stress relaxation tests for five different strain rates ($15\%/min, 25\%/min, 30\%/min, 300\%/min$ and $500\%/min$) using a ramp strain -15%. Four scaffolds with 10% PEGDA were tested (n=4).

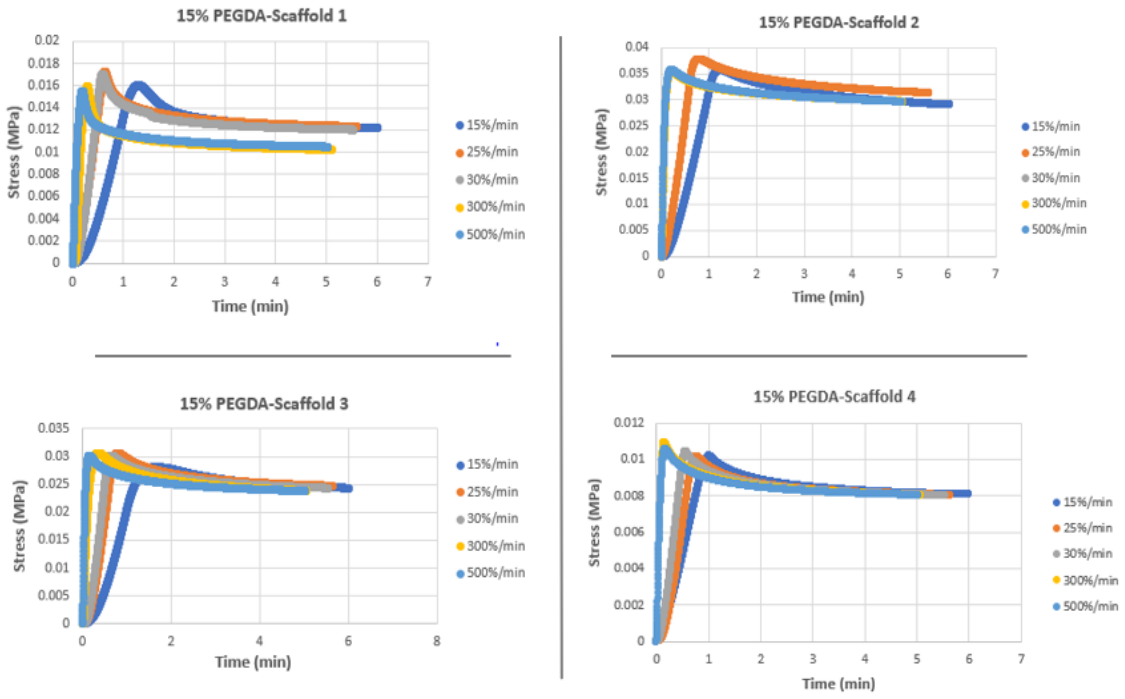

Figure 3.12: Stress-Time curves of scaffolds made from bioink with 15% PEGDA, after the performance of stress relaxation tests for five different strain rates ($15\%/min, 25\%/min, 30\%/min, 300\%/min$ and $500\%/min$) using a ramp strain -15%. Four scaffolds with 15% PEGDA were tested (n=4).

Figure 3.13 demonstrates the results from the mechanical characterization of the printed scaffolds, which were subjected to stress-relaxation tests with five different strain rates. It can be generally said that the response of scaffolds in terms of their mechanical behavior is similar to that observed for the discs (characterization of the bulk material properties). The main difference is related with the fact that the equilibrium modulus, as well as, the values of the maximum and equilibrium stress are significantly lower in the case of the scaffolds, a fact which is totally justifiable taking under consideration the differences in architecture. The equilibrium modulus of the scaffolds made from 10% PEGDA ($0.065 \pm 0.0014MPa$) is quite lower for the scaffolds made from 15% PEGDA ($0.12 \pm 0.003MPa$). The same pattern is observed for the max and equilibrium stresses, where max stress is 0.012 and $0.023MPa$ for 10% and 15%PEGDA, while the equilibrium stress is 0.009 and $0.018MPa$ for 10% and 15% PEGDA,

respectively. These differences are attributed to the increased crosslinking efficiency of the bioinks with 15% PEGDA. In terms of relaxation, lower percentages appeared in general for the bioinks with 15% PEGDA ($\simeq 74.9\%$ at max) compared to the 10% PEGDA ($\simeq 82.7\%$ at max). This concept was the same also for the bulk materials. As far as the differences between the tested strain rates, for scaffolds made with the same bioink, no significant variation was observed in any of the graphs.

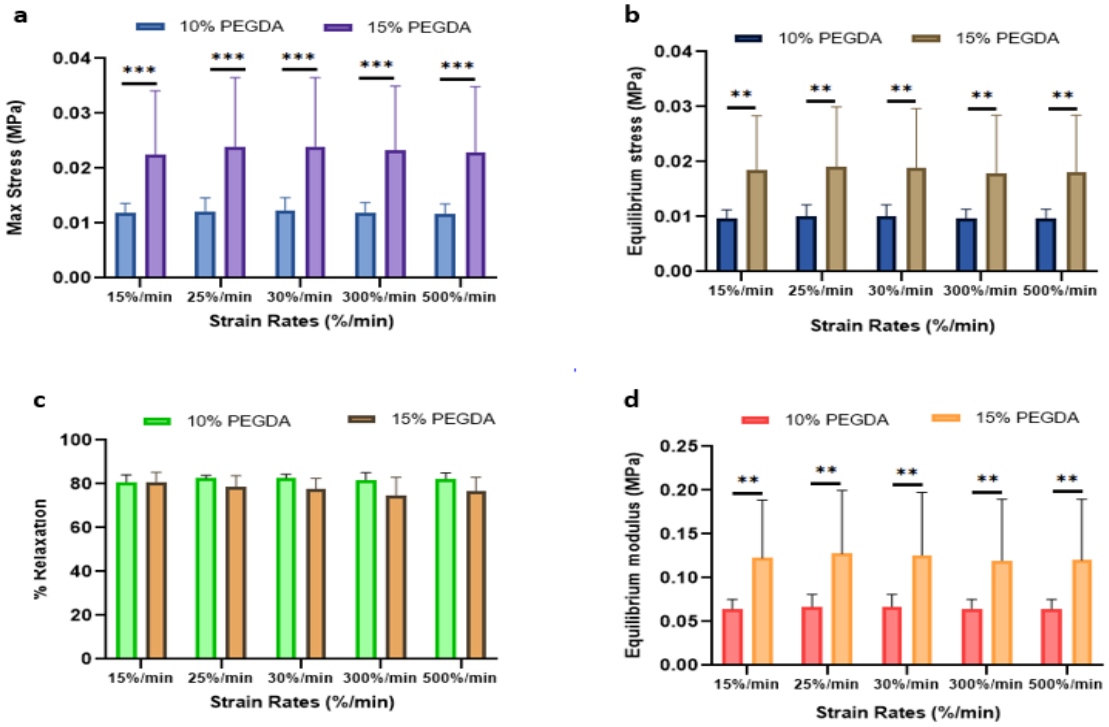

Figure 3.13: Results from the mechanical characterization of scaffolds made from the final optimal bioinks with 10% and 15% PEGDA). The maximum (a) and equilibrium (b) stress, as well as, the percentage of relaxation (c) and the equilibrium modulus (d) are presented for each of the five different strain rates and directly compared between the two bioinks. The data are expressed as mean $\pm$ standard deviation ($n = 4$, * for $p < 0,05$, ** for $p < 0,01$, *** for $p < 0,001$ and **** for $p < 0,0001$).

3.5 Cell viability and proliferation tests for bioprinted and post-seeded hydrogel scaffolds

3.5.1 Live/Dead Assay

The performance of the Live/Dead Assay for the days 2 and 7 of culture, resulted in the graph of **Figure 3.14** , which can give an estimation of the cell viability for each of the different scaffold conditions. Particularly, both of the seeded scaffolds made from the bioinks with 10% and 15% PEGDA, have significantly higher percentages of cell viability compared to the bioprinted scaffolds were the cells where encapsulated in the bioinks. Moreover, the percentages of cell viability appeared to be increased at the 7th day of culture comparing to the 2nd, for all the scaffold conditions, except from the bioprinted scaffold with 15% PEGDA, where there is a slight decrease. These conclusions can be also confirmed from **Figure 3.15**, where live/dead images of MSCs from all the tested hydrogel scaffolds conditions are demonstrated.

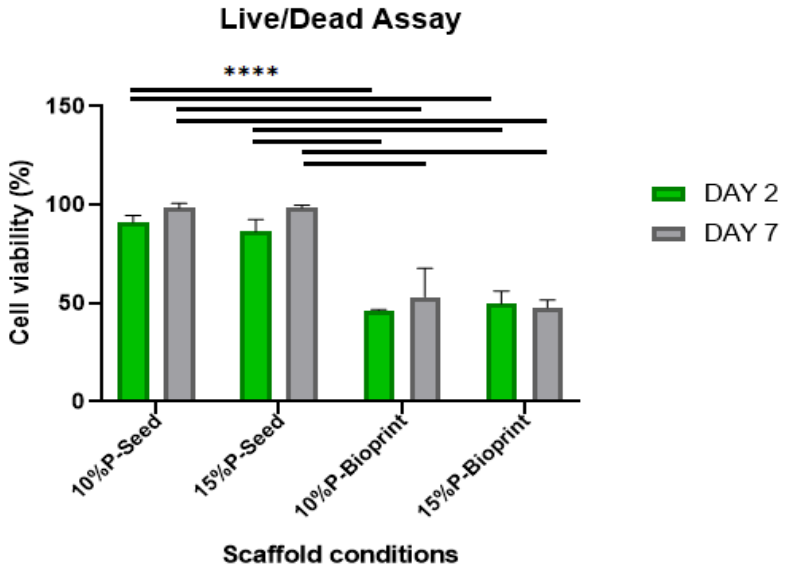

Figure 3.14: Results from Live/Dead Assay. The percentage of cell viability is demonstrated for the four different scaffold conditions, corresponding to the seeded scaffolds made from 10% and 15% PEGDA, as well as the bioprinted scaffolds from 10% and 15% PEGDA. The viability was tested for the days 2 and 7 of the culture. The data are expressed as mean $\pm$ standard deviation ($n = 4$, * for $p < 0,05$, ** for $p < 0,01$, *** for $p < 0,001$ and **** for $p < 0,0001$).

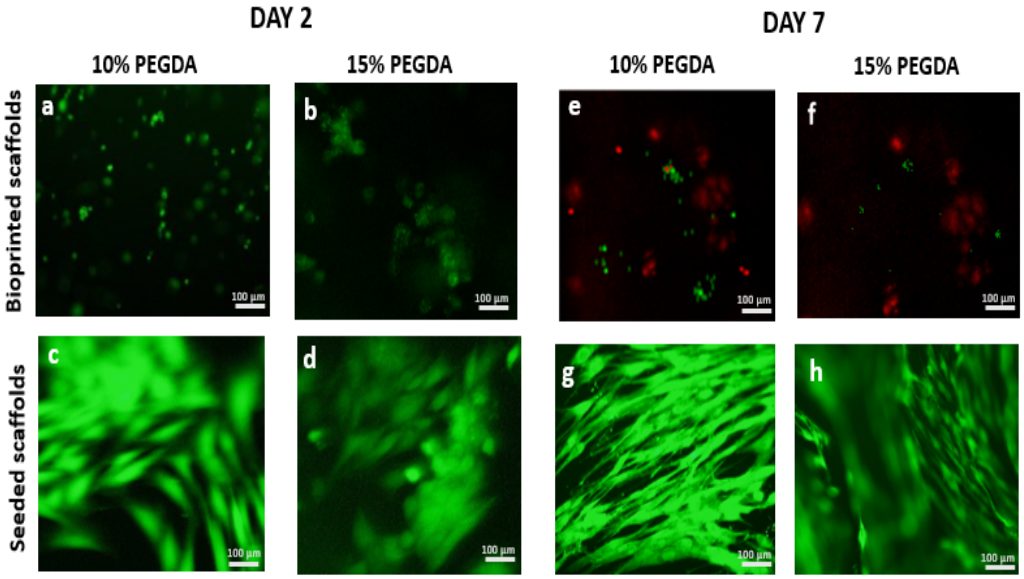

Figure 3.15: Live/dead images of MSCs from all the tested hydrogel scaffolds conditions: (a,b) Bioprinted scaffolds from 10% and 15% PEGDA bioink at day culture 2, correspondingly. (c,d) Seeded scaffolds from 10% and 15% PEGDA bioink at day culture 2, correspondingly. (e,f) Bioprinted scaffolds from 10% and 15% PEGDA bioink at day culture 7, correspondingly. (g,h) Seeded scaffolds from 10% and 15% PEGDA bioink at day culture 7, correspondingly. Pictures were taken at the upright fluorescence microscope, 10x magnification. Live=Green, Dead=Red. Four gels per condition were tested ($n = 4$).

3.5.2 Alamar Blue Assay

The cell proliferation of the bioprinted and post-seeded hydrogel scaffolds was investigated through the Alamar Blue Assay. The plot of the relative fluorescent units, as occurred from the fluorescent reader-plate for each of the different time points that the samples were tested (Day 1, 4, 7 and 10) can be observed at the graph of **Figure 3.16** . It seems that the cells in the bioprinted scaffolds did not have the chance to proliferate and by day 10 probably they have started to dye. However, the cells at the post-seeded scaffolds showed signs of cell proliferation demonstrating higher values of relative fluorescent units. This behavior could be observed because when added to cells, the alamar blue reagent, is modified by the reducing environment of viable cells and turns into a red highly fluorescent color. For days 1 and 4, no difference can be seen for both the 10% and 15%

PEGDA seeded scaffolds. However, from day 7, the 10% PEGDA seeded scaffolds start to show better results of cell proliferation compared to 15% PEGDA.

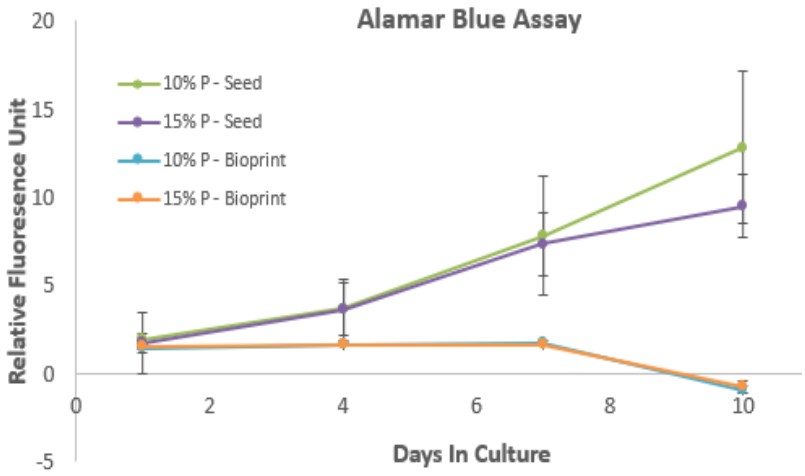

Figure 3.16: Results from Alamar Blue Assay. Plot of the relative fluorescent units for each of the tested days in culture (Day 1, 4, 7 and 10), as it was produced from the performance of the Alamar Blue Assay. The data are expressed as mean $\pm$ standard deviation ($n = 4$).

Chapter 4

Discussion

4.1 Choice of resin components

The first step of the research is based on the proper selection of the materials, which is critical for the development of an optimal bioresin.

- Hybrid system
  -Gelatins are formed from the partial hydrolysis of collagen, which constitutes one the primary components of the ECM for most of the animal tissues. They have plentiful arginine-glycine-aspartic acid(RGD) sequences that support cell attachment, as well as, sequences of matrix metalloproteinases (MMP), which promote ECM remodeling [63,64]. Gelatins, as denatured collagens, are characterized from low antigenicity, high solubility and a low gelling point, but they have also low mechanical modulus and undergo rapid degradation [63, 65, 66]. To compensate these disadvantageous properties, chemically modified gelatin (GelMA) was developed and used for the creation of photopolymerized hydrogels under the exposure to light in the presence of a photoinitiator. However, one of the main drawbacks of GelMA is the insufficient stiffness which renders the control of matrix's rigidity.

  - Poly(ethylene glycol) diacrylate (PEGDA) is another biocompatible material approved by the Food and Drug Administration, which have been widely used in the field of regenerative medicine [68]. High molecular weight PEGDA ($Mn > 2000gmol - 1$) has been typically used for cell encapsulation since the resulting hydrogels have lower crosslinking density

allowing cells to proliferate and migrate [69, 70]. Low molecular weight PEGDA ($Mn = 250gmol - 1$) has been used from other researchers for the development of microfluidic devices resisting to swelling and impermeable to water [71,72]. Since one of the goals of the present study was the creation of bioprinted scaffolds with structural integrity, an intermediate value of molecular weight ($Mn = 700gmol - 1$) PEGDA was selected to print mechanically stable, but yet diffusion-open and compliant structures. Additionally, PEGDA ($Mn = 700gmol - 1$) is commercially available at a much lower price compared to its counterparts with higher Mn.

Consequently, in an effort to strike the right balance between enhanced cell attachment and adequate mechanical strength, the combination of GelMA and PEGDA was decided for the development of a promising bioink.

- Photoinitiator
  The choice of photoinitiator in light-based bioprintig is crucial since its absorption peak prescribes the wavelength of light that must be applied to the bioink. Several studies have demonstrated a direct impact of this wavelength to the cell viability. Particularly, the ultraviolet A radiation (UVA, wavelength $320400nm$) can impair the cells' nuclear DNA leading to genomic mutations or carcinogenesis [73, 74], or Ultraviolet B (UVB, wavelength $290320nm$) can induce cell apoptosis [75]. For this reason, researches have tried to investigate the use of visible light photoinitiators, such as ru/SPS [76, 77].

  The commercial printer, which was used in the present study (Atum3D), had a light source with wavelength at $405nm$, which is blue light, classified as visible. Despite its operating quite close to the UVA, it is expected that it will not have adverse effects on cell viability. LAP, a water soluble, cytocompatible photoiniator was used in the synthesis of the bioink. LAP is, in general, preferable over other photoiniators, like Irgacure 2959 for biological applications, due to its increased water solubility, increased polymerization rates with 365 nm light, and absorbance at 400 nm allowing for polymerization with visible light [78].

- Photoabsorber
  Curing depth is one of the key parameters of photocrosslinkable materials, which has to be controlled in such a way that the light will not penetrate too deep into the preceding printed layer creating undesired features (overcuring). To avoid this issue, a possible increase in the photoinitiator's

concentration could be performed in order to increase the absorption of the resin and reduce the cure depth. However, this method is not preffered, not only due to the increase of crosslinking densities, but also due to the possible cytotoxity of the initiator. For these reasons, non-reactive photoabsorbers are preffered to reduce the light penetration and increase the printing resolution especially in the z-direction [79, 80]. In the specific bioink, yellow food dye (Queen Fine Foods, Australia) was chosen as an efficient photoabsorber.

4.2 Printing optimization of hydrogel bioinks

The problem of the stereolithographic printing resolution, in general, is directly connected with the difficulty in tuning the light penetration depth. As it has been earlier discussed, deep light penetration depth ensures the bonding between subsequent layers since the light penetrates to the previously printed layers, however, it can also lead to overcuring resulting in decreased vertical dimensions and clogged channels (**Figure 2.3**). To avoid this problem, the use of a photoabsorber has been proven extremely valuable in the synthesis of a photo-sensitive ink since it can control the light penetration depth and match it properly with the layer thickness.

For the optimization of bioinks' synthesis in terms of resolution, as well as, the definition of printing parameters, the working curves of all the tested hydrogel conditions were evaluated in an effort to study their curing properties. Three graphs in total were plotted corresponding to three different PEGDA concentrations. The assessment started with the working curve corresponding to 10% PEGDA, since it was the intermediate PEGDA concentration and could be used as a guideline for finding faster and more effectively the optimal printing settings for the bioinks with 5% and 15% PEGDA.

After the construction of the working curve for 10% PEGDA and three different photoabsorber concentrations (2%, 2.5% and 2.7% yellow dye), the critical energy and light penetration depth for each of these conditions were studied. Taking under consideration the requirement of printing mechanically stable structures with adequate resolution, prospective optimal values for the photoabsorber concentration, as well as, the energy exposure and layer thickness were hypothesized based on the assessment of the working curves, as it has been thoroughly described in the Section 3.1.3 (Test cube design print). Consequently, the printing results using the hypothesized conditions will indicate what kind of

changes are required in order to find the optimal conditions. For example, the conditions used for the print of Figure 3.4b resulted in an incomplete cube due to the insufficient crosslinking density of the bioink. To overcome this problem, the exposure time of light on the bioink was increased in an effort to increase the crosslinking efficiency. However, this change resulted to the creation of an overcured cube with clogged channel. This means that light penetration depth had to be reduced. One of the ways to achieve that is by reducing the energy exposure from 100% to 80%. Since this change would affect the curing depth, the layer thickness of the printer had to be adjusted following the rule of thumb. According to this, the layer thickness should be approximately half of the cure depth, as it has been measured for the development of the working curve, in order to ensure a strong bonding between neighboring layers. However, since this rule of thumb is a rough estimation, several prints with slight changes in the layer thickness were created, until the finding of the optimal thickness, which was 80 μm in the present study. Based on this procedure, the optimal bioink with 10% PEGDA was consisting also from 10% GelMA, 0.2% LAP and 2.7% dye, while the optimal printing parameters were 80% light intensity, 80 μm layer thickness and 3 sec time exposure.

The discovery of the optimal bioink with 15% and 5% PEGDA, as well as, the definition of the printer parameters, were based mainly on the findings for the bioink with 10% PEGDA. Particularly, the increase in PEGDA concentration increased the crosslinking efficiency, as can be observed from the increase of cure depths comparing bioinks with the same photoabsorber concentration. For this reason, the same concentration of yellow dye was used for the synthesis of the bioink with 15% PEGDA (2.7%), but the time exposure was reduced from 3 to 2 sec in order to eliminate the crosslinking efficiency. On the contrary, for bioinks with 5%PEGDA, the time exposure was increased from 3 to 4 sec, since the reduction of the PEGDA concentration, reduced the crosslinking efficiency. In the case of the 5%PEGDA bioink, the photoabsorber concentration had to be also reduced from 2.7 to 2.5% in order to avoid the creation of slightly distorted cubes due to poor crosslinking efficiency.

After the successful print of the first test cube design, further examination for the spatial resolution of the printing set up was performed. This investigation demonstrated the difficulty in printing constructs with small dimensions and especially channels with diameters physiologically relevant (diameters smaller than 500 μm) [59,60].

The spatial resolution was examined for all of the three optimal bioinks, as they have been selected after the study of their working curves, critical energy

and light penetration depth (See section 3.1.3).

Particularly, positive and negative features were fabricated with these bioinks and consequently, the printed dimensions were compared to the designed ones. For the bioinks with 5% PEGDA, almost all the positive features could not be measured since the pillars collapsed. As far as the negative features, even though channels with cross-section as small as 500 μm x 500 μm were created, the perfusion of the channels was achieved only for those with $750\mu m$ diameter. In general, the prints produced with the bioink consisting of 5% PEGDA, were quite soft and prone to collapsing. Since, one of the main goals of the present study was the print of robust, mechanically stable scaffolds, this bioink was excluded from any further investigation.

As far as the bioink with 10% PEGDA, the dimensions of the designed and printed positive features were quite similar, with a small difference only for the pillar with 1000 μm. Quite similar were also both the vertical and horizontal dimensions of the printed negatived features compared to the designed ones using a 2.7% concentration of dye and layer thickness of 80 μm . However, only channels with diameter about 750 μm were able to be created and perfused. An increase in the dye concentration to 2.9% was attempted, in an effort to reduce the light penetration depth and increase the printing resolution of the negative features, however it ended up in a slightly distorted print. For this reason, the 2.7% concentration was kept as an optimal photoabsorber concentration for the bioink with 10% PEGDA.

For the bioink with 15% PEGDA and 2.7% dye, almost all the positive features were printed having dimensions quite similar to the designed ones. After comparing the negatives features, it seems that the increase in PEGDA concentration promoted significantly, the printing resolution, since channels up to approximately 100 μm were printed and up to 500 μm successfully perfused. For this reason, the bioink with 15% PEGDA and 2.7% dye, was kept as optimal.

Even though the bioink with the highest PEGDA concentration (15%) was the one resulting in higher printing resolution, the bioink with 10% PEGDA was also tested at the remaining part of the present study, since in general, the lower crosslinking density leads to the production of less stiff hydrogels, which are more suitable for cell encapsulation.

4.3 Characterization of final optimal hydrogel bioinks

4.3.1 Problems with Atum3D printer and re-optimization of bioinks

As it has been mentioned earlier, despite the successful printing optimization of two bioinks (with 10% and 15% PEGDA), after a certain time point, the printer stopped to fabricate well-defined prints. Particularly, even though the exact same previously optimized bioinks and printing properties were used, only incomplete prints were fabricated. The prints were incomplete since during the printing process, they were detaching from the building.

In order to solve the problem, all the parameters that could possibly affect the printing procedure were investigated. Starting with the printer, the check of building plate for any defect, the change of the base plate with a new one, the performance of a diagnostic test, as well as, the calibration of the printer did not show any evidence of malfunction. Moreover, the performance of prints using commercial resins confirmed that the printer is working properly and the problem is possibly related with the bioinks. The detachment of prints from the building plate indicated that the bioinks have lost their crosslinking efficiency. In order to resolve this issue, several solutions were tried. As far as the setting of the printing properties, the increase of curing time for the initial printing layer, or the increase of initial layers with higher exposure time (in order to ensure the attachment of the print to the building plate) were attempted. The decrease of the optimized layer thickness from 80 μm to 70 and 60 μm, as well as, the increase of light intensity from 80% to 90% and 100%, in order to ensure a stronger bonding between subsequent layers, were also unsuccessfully performed. Changes were also performed to the retraction height (=amount of retraction that is needed for the material to be released from the VAT in mm) since during the optimization process, this height had been decreased from 5 to 0.5 mm decreasing also drastically the printing time. The change of the retraction height seemed not to play any important role in preventing the collapse of prints until the point where the photoabsorber concentration was reduced. Particularly, a dramatic decrease of the dye concentration from 2.7% to 1.2% and 1.4%, for the bioinks with 10% and 15% PEGDA, had to be performed in order to achieve the fabrication of complete structures with decent resolution. The rest of components' concentrations and printing properties remained the same, except from the retraction height, which was increased from the optimal value of 0.5 to 1 in order to avoid the printing of scaffolds with distorted architecture. As far

as the changes in bioinks' synthesis, the increase of photoinitiator (LAP) from 0.2% to 0.3% led to the creation of a complete structure in the case of the bioink with 15% PEGDA, but the printing resolution was poor.

In order to overcome the problem of prints' detachment from the bare building plate, the creation of an initial hydrogel layer on the surface of the building plate, prior the fabrication process, was also attempted, using the same hydrogel precursor solution and a UV light source. It was hypothesized that this layer could possibly create a base on top of which the print would have better chances of attachment, however it did not work either.

In an effort to figure out, which component of the bioink could create these problems, the crosslinking efficiency of GelMA was tested. Particularly, a precursor solution made from 10% GelMA and 0.2% LAP, was pipetted inside a Teflon mold air tightly covered with glass slide and placed in a UV oven for 15 min. The obtained gels were crosslinked, but quite weak and brittle, even though any photoabsorber was used. Consequently, the possible degradation of GelMA with the pass of time could be an explanation for the unsuccessful printing trials taking also under consideration that the rest of the components were recently purchased. Several trials were performed using GelMA from different tubes of the same batch, which was specifically prepared for the present research study, but also from other older batches. In any case, the dramatic reduction of the photoabsorber concentration was required, in order to print complete structures. However, this reduction eliminated significantly the printing resolution, while even the slight increase of dye ($\approx 0.1\%$) could lead to incomplete prints due to insufficient crosslinking.

It is worth mentioning that the tubes with GelMA were stored in 4 °C prior to use, having filter lids that are covered with paraffin wax. This is attributed to the fact that the last step of GelMA synthesis, is the freeze-drying procedure, which requires the use of tubes with such lids. However, it is possible that the covering of lids with paraffin wax is not sufficient to protect GelMA from the humidity, while is stored in fridge for an extended period of time. Hence, the change of filter lids with solid ones, could be proven beneficial to the life expectancy of GelMA.

Finally, another less obvious reason, which could hamper the successful DLP printing of hydrogel scaffolds, is related with potential environmental implications. Particularly, the experiments for optimizing the printing resolution of the bioinks started at the end of spring and by the end of summer, hydrogel structures with mechanical stability and high resolution (up to $\approx 100\mu m$ for positive features and $\approx 500\mu m$ for negative features) were fabricated. However, by

the end of September, where the weather was cooler, the previously optimized bioinks could not produce complete structures. A similar pattern of unsuccessful printings using the same DLP printers, had been observed one year ago in the laboratory (see Appendix A1). Since the printers did not have a system of controlling environmental conditions, a few attempts were performed to imitate the environmental conditions during summer. Particularly, all the components of the bioink were pre-warmed at 37°C, a hair dryer was used to warm the chamber of the printer and two beakers with hot water were placed inside the chamber in an effort to keep a certain level of humidity. Unfortunately, none of these attempts helped in the successful fabrication of structures with the previously optimized bioinks.

However, during the performance of the aforementioned trials to resolve the problems with the Atum3D printer, a few porous scaffolds with decent resolution were created after the re-optimization of the bioinks. This re-optimization involved a significant decrease of the photoabsorber concentration (yellow dye) in order to increase the crosslinking density and avoid the collapsing of the prints from the building plate. The printing properties remained the same with the original ones and the final optimized bioinks, which were characterized in terms of crosslinking efficiency and mechanical properties were the following:

- Bioink 1: 10%PEGDA, 10% GelMA, 0.2% LAP and 1.2% yellow dye.
- Bioink 2: 15% PEGDA, 10% GelMA, 0.2% LAP and 1.4% yellow dye.

4.3.2 Crosslinking efficiency

Photocrosslinkable hydrogels are highly used for tissue engineering applications, because their properties (swelling ratio, stiffness) can be tuned allowing high cell viability [81]. Sol-gel studies were performed in order to evaluate the physico-mechanical properties of hydrogel discs made from the two final re-optimized bioinks using DLP. The results showed that the hydrogels made from the Bioink 2 (15% PEGDA), had significantly higher gel content (% macromer) due to the higher concentration of PEGDA. This parameter is reversely proportional to the swelling ratio, which was higher in the hydrogels made from 10% PEGDA. In general, the swelling ratio constitutes an important parameter in the tissue engineering field, since it can affect surface properties or solute diffusion. It is dependent on the interaction between polymer and solvent, as well as, the pore size of polymer [82]. From the results, it can be observed that as the hydrogel content increases with the density of the networks generated,

its swelling capacity decreases. Comparing the swelling ratio of hydrogels made only from 10% GelMA (≈ 10) to the corresponding ratio of the tested hydrogels, made from 10% GelMA plus 10% or 15% PEGDA, a significant reduce can be observed (≈ 5.7 and 4.7, respectively). This decrease in swelling ratio, as a result of the increased gel content and thus, crosskinking density can adversely affect the cell viability, as it would be later explained.

4.3.3 Mechanical properties of bulk materials

As it has been earlier discussed, hydrogels are often the material of choice for several applications in the field of biomedical engineering. One of the main reasons is related with their resemblance to the ECM of many tissues.

It has been well known that the ECM in all the biological tissues (even the hard ones), are viscoelastic [83–85]. This means that they have a time-dependent response upon deformation or loading, displaying stress relaxation or creep, correspondingly.

In the present study, the mechanical properties of the hydrogel bioinks were tested in terms of their stress relaxation behavior under the application of a ramp strain up to -15% (ϵ_0) for five different strain rates ($15\%/min, 25\%/min, 30\%/min$, $300\%/min$ and $500\%/min$).

During the performance of stress relaxation tests, the discs were suddenly deformed at a certain strain ϵ_0 and the resulting stress was measured as a function of time. The relationship between the measured stress and the fixed strain following the equation (4.1) defines the relaxation modulus $G(t)$.

$$G(t) = \frac{\sigma(t)}{\epsilon_0} \tag{4.1}$$

As can be observed from the corresponding stress-time curves, while the strain is kept fixed, the resulting stress reached a point of equilibrium after a certain amount of time. At this point, the compressive equilibrium modulus can be determined using the equation (4.1), where the value σ can be defined from the last data point of the test. The measurement of this equilibrium modulus, is quite important, since it constitutes a measurement of the intrinsic stiffness of the hydrogels. It is worth mentioning that the equilibrium modulus, is different from the "instantaneous" modulus, which refers to the initial elastic response and is highly dependent on the strain rate. On the contrary, the equilibrium modulus is a material property and for this reason remains the same independently the strain rate. As can be seen in **Figure 3.9(d)**, the equilibrium modulus is approximately

$0.25 \pm 0.008 MPa$ for the discs with 10% PEGDA and $0.6 \pm 0.01 MPa$ for the discs with 15% PEGDA. Consequently, the discs with 15% PEGDA are stiffer than those with 10%, as it was expected, due to the higher crosslinking efficiency of hydrogels with increased PEGDA concentration.

This conclusion can be confirmed also from the graph of **Figure 3.9(c)**, which demonstrates the percentage of relaxation calculated from the ratio of equilibrium stress with the maximum one. Particularly, it seems that the relaxation response is smaller in the case of hydrogels with 15% PEGDA, as it was expected, since they are stiffer than the hydrogels with 10% PEGDA.

As far as the equilibrium and peak (max) stresses, even though there is significant deviation between the two hydrogels, no significant difference could be observed between the different strain rates (for the same hydrogels). Since it is hypothesized that the hydrogels exhibit viscoelastic behavior, it would be expected that as the strain rate increases, the maximum and equilibrium stress will also increase. In other words, it would be expected an upward shift of the stress-time curves, which corresponds to higher strain rates. (The performance of test with an even higher strain rate in order to further investigate the expected behavior, was not possible due to the limitation of the DMA machine - max strain rate $500\%/min$.)

In order to understand and explain this observation, it is important to delve a bit deeper into the principles of viscoelasticity.

Viscoelasticity, as the name suggests, is the property of materials to exhibit both viscous and elastic characteristics under deformation. The term "viscous" insinuates a slow deformation of the materials when exposed to an external force. In other words, viscous materials, like water, resist shear flow and strain linearly with time, while elastic materials immediately return to their original configuration once an external force is removed [86]. Viscoelastic materials have elements of both of these properties and, as such, exhibit time-dependent strain.

Several models have been created using linear combinations of springs and dashpots, in order to describe the linear and viscous components of the viscoelastic materials, correspondingly [87, 88].

Even though these models have been widely used for the description of viscoelastic behavior, they fail to describe the known effects of interstitial fluid flow, which is crucial for the appropriate description of tissues' viscoelastic behavior. Early studies demonstrated that when a tissue is compressed it will loose water, while, when is soaked in fluid, it will absorb water [89, 90]. One of the most successful theories to describe this behavior has been created by Mow and coworkers and is called biphasic theory [91–93]. According to this, soft hydrated

tissues are modeled as composites materials consisting of two intrinsically incompressible and immiscible phases (a solid and a liquid). The porous solid phase is elastic and permeable, while the frictional drag associated with the interstitial fluid though the porous solid matrix is responsible for the viscoelastic behavior of the tissue.

The same theory, can be applied in the case of the hydrogels, which are three-dimensional networks of crosslinked hydrophilic polymers having a porous solid matrix, as well as, water content. The frictional drag of the water though the porous matrix of the hydrogel is responsible for the hydrogel's viscoelastic behavior.

The fact that in the present study, the tested hydrogels do not demonstrate the expected viscoelastic response (higher max stress for higher strain rates) indicates that probably there is low water content in the hydrogels. Consequently, the mechanical behavior represented in the stress-time curves is mainly due to the response of the hydrogel's porous matrix (which according to the biphasic theory is elastic). This characteristic along with the lack of proper osmosis within the hydrogel matrix deprive the tested hydrogels of the opportunity to resemble closer the ECM of natural tissues.

4.4 Characterization of scaffolds' mechanical performance

The results from the mechanical characterization of the printed scaffolds demonstrate similar behavioral patterns with these exhibited from the characterization of the bulk material properties. Particularly, the equilibrium modulus, or in other words the stiffness of scaffolds with 15% PEGDA is almost double ($0.12MPa$) than this of the scaffolds 10% PEGDA ($0.065MPa$). This result was expected since hydrogels with increased concentration of PEGDA have also increased crosslinking density and thus, stiffness. Consequently, the scaffolds made from bioink with 15% PEGDA, demonstrate higher values of max stress and equilibrium stress compared to these made from 10% PEGDA. However, both of the stress values found for the scaffolds, are significantly lower than the corresponding ones found for the discs. This is explained from the fact that the discs were solid, while the scaffolds were porous (with $\approx 77\%$ porosity). It is obvious that the introduction of pores to the architecture reduces the stiffness and possibly the mechanical stability of the scaffolds, however adequate porosity is one of the requirements for successful biofabrication of tissues.

It is worth mentioning that at the stress-time curves of the scaffolds made from both 10% and 15% PEGDA (**Figures 3.11 and 3.12**), the viscoelastic response is more prominent compared to the discs (**Figure 3.7 and 3.8**). However, as it has been earlier mentioned, the viscoelastic behavior is the result of the frictional drag of water though the porous hydrogel matrix. In the case of the tested scaffolds, it is speculated that this more prominent viscoelastic response is the result of frictional drug created from the water existing in the holes and surfaces of the scaffolds itself upon compression.

Finally, it is observed that the scaffolds with 15% PEGDA, demonstrate results with quite high standard deviations, while the stress-time curves have also differences (**Figure 3.12, 3.13**). This could be explained from the fact that even though the scaffolds had decent resolution, they were fabricated with a probably degraded bioink. As it has been mentioned earlier, at some point during the conduction of research, the Atum3D printer started to have difficulties in creating complete structures with the originally optimized bioinks. This issue was attributed to either environmentally implications, or to degradation of GelMA. The use of a problematic component in the bioink synthesis could possibly lead to inconsistent results.

4.5 Characterization of scaffolds' biological performance

The results of live/dead assay by day 2 of cell culture showed high cell viability for the seeded scaffolds made from both 10% and 15% PEGDA ($\approx 91\%$ and 86%, accordingly). However, the cell viability of the bioprinted scaffolds was about half reduced. By day 7, the viability of the seeded scaffolds had increased up to $\approx 98\%$, while a small increase of about 10% was observed also for the 10% PEGDA bioprinted scaffolds. However, their viability percentages were still significantly lower than these of the seeded scaffolds.

The performance of Alamar Blue assay showed any sign of cell proliferation for the cells, which were encapsulated in the bioinks both with 10% and 15% PEGDA. By day 10, it seems that they have already die. This could possibly happen due to the high crosslinking density of the hydrogels, since too stiff hydrogels do not allow cells to migrate into it and the ECM that they release stays confined around the cells instead of spreading all over the gel. However, the proliferation of cells seeded on the surface of scaffolds was gradually increased up to day 10, where the scaffold with 10% PEGDA seemed to offer a bit better

substrate for the cells.

In any case, the cell viability and proliferation experiments demonstrated that the developed bioinks were not suitable for cell encapsulation. However they constitute an exceptional material for the creation of post-seeded scaffolds. The ability of MSCs to attach, expand and proliferate on top of the scaffolds' surface (for both conditions with 10% and 15% PEGDA) can be observed in **Figure 3.15(c,d,g and f)**.

However, at this point, it is worth mentioning that these results could be affected from the possible degradation of GelMA, as it has been earlier mentioned. The addition of 10% GeLMA to the final bioink, was originally decided, since quite a few studies have reported successful encapsulation of different cell types in GelMA hydrogels [96–98]. On the other hand, pure PEGDA hydrogels demonstrate poor viability for long term culture of encapsulated cells, especially at high polymer concentrations [94].

Chapter 5

Conclusions and Future Outlook

Although at an early stage of development, continuous advancements in DLP bioprinting have been accomplished allowing the creation biofabrication systems with a variety of biomaterials and cells, in an effort to meet specific requirements for the successful development of functional tissues. However, there are still important barriers that overshadow the wide spectrum of DLP bioprinting applications and need to be addressed. Many of these challenges lie at key components and the complexity of bioink preparation is one of them.

Hydrogel bioinks appear as promising materials for the bioprinting technology, however, they create difficulties in the light-based printing of complex structures, which will be cell-friendly, but will have adequate mechanical stability at the same time.

For this reason, the development of a hybrid bioink composed from PEGDA and GelMA was decided. PEGDA, as a synthetic hydrogel, could offer the opportunity of tuning the mechanical properties, while GelMA, as a semi-natural hydrogel, will add to the biocompatibility of the bioink. LAP, a water soluble, cytocompatible and low toxicity photoinitiator was included into the bioink, as well as, a photoabsorber in the form of yellow food dye. The careful choice of the components developed a system with promising characteristics.

The first step towards the realization of printing structures is the optimization of printing resolution. This process is quite challenging and far from trivial in order to achieve the fabrication of constructs with mechanical integrity and fidelity. The reason behind this is related with the fact that the printing resolution is based on multiple factors. Some of the most important include the type and concentration of the bioink's monomer, photoinitiator and photoabsorber, as well as the light intensity, the time exposure and the layer thickness. The

bioresin optimization in terms of printing resolution constituted a major part of the present study. The originally optimized bioinks achieved a printing resolution up to $100\mu m$ for positve features and up to $500\mu m$ for negative features (perfusable channel). However, after a certain point, due to possible degradation of GelMA, or environmental implications at the lab, the DLP printer stopped to produce the previously achievable high resolution constructs. Instead, all the prints were incomplete due to their detachment from the building plate during the fabrication process. After the performance of several trials in order to resolve the problem, the bioinks were re-optimized in terms of printing resolution since they were able to produce an intricate structure with $700\mu m$ pore diameter and decent resolution. The final two re-optimized bioinks with two different concentrations of PEGDA were characterized in terms of their crosslinking efficiency and mechanical properties. It was demonstrated that the bioink with higher PEGDA concentration (15%), had higher gel content, lower swelling ratio and also higher stiffness ($0.6MPa$), compared to the bioink with 10% PEGDA ($0.25MPa$). These differences in the bulk material properties of the bioinks were reflected also to the fabricated scaffolds, where the 15% PEGDA scaffolds had an equilibrium modulus (intrinsic stiffness) $0.12MPa$, while the 10%PEGDA ($0.06MPa$). As far as the characterization of the scaffolds in terms of biological performance, it was shown that both final bioinks were not suitable for long term cell encapsulation, since by day 10 of culture, the cells had died. On the contrary, the post-seeded scaffolds demonstrated high cell viability up to 98% for both conditions at day 7 of culture. In case that the GelMA component had degraded, the experiments for the characterization of the bioinks should be repeated after the synthesis of fresh GelMA (in small batches). If even after the repetition of experiments, there is no significant improvement in the biological performance of the encapsulated cells, the bioink with higher concentration of PEGDA should be chosen as optimal, since it would produce stiffer and probably higher resolution prints, while the viability of cells would probably remained unaffected, or slightly changed, since the cells would be seeded on the scaffold (-and not encapsulated, where a less stiff/compact hydrogel matrix would be required for cell proliferation).

From the present study, it is shown that the changes in PEGDA concentration can really tune the mechanical properties of the bioinks and their corresponding scaffolds from a physico-chemical point of view. However, another factor, which has been hardly investigated and can also lead to fabrication of hydrogel scaffolds with tunable mechanical properties, is the actual design of the scaffold. Once the problem of printing resolution is solved, the DLP technology permits the fabrication of complex architectures with exceptional accuracy and can be used for

the creation of scaffolds with well-defined pores, pore interconnectivity, distribution or gradients. It is worth mentioning that the introduction of open pores and interconnectivity in printed scaffolds is crucial for cells' nutrition, proliferation, migration, as well as, the vascularization and tissue formation [99–101]. However, an increased porosity can often compromise the mechanical stability. For this reason, a counterbalance between mass transport and mechanical function should be adopted for the development of an optimal scaffold system. The orientation of future studies into combining the use of hydrogel bioinks for the fabrication of scaffolds with specific design requirements can possibly lead to the successful development of soft tissues with several applications in regenerative medicine.

Acknowledgments

I owe my deepest gratitude to my supervisor Prof Harrie Weinans for providing me his invaluable support and encouragement throughout the course of the project. I would like also to express my special thanks of gratitude to my daily supervisor Dr. Riccardo Levato for his constant guidance and support in order to achieve the scientific skills and mindset required in the field of biomedical engineering. Finally, I would like to thank my technical supervisor Ms. Anneloes Mesinga without whom gaining lab experience would have been a difficult journey and Prof Jos Malda for allowing me to carry out my study in his department.

Appendix

A1. Preliminary experiments

Prior to the final choice of the components, which were used for the synthesis of the optimal bioink consisting of GelMA, PEGDA, LAP and yellow food dye, a few experiments had been conducted testing other possible bioinks. For the printing of complex structures with high fidelity via the DLP stereolithography method, the printing parameters need to be optimized. In order to achieve this target, the working curves for the desired bioinks had to be constructed.

Preliminary Test 1

- Printer: Atum3D
- Tested bioink A: 10% GelMA + 0.2%LAP + Different yellow dye concentrations varying from 0 to 0.2%, 0.5% and 1%
- Working curves: Development of graphs (Figure 5.1) following the procedure thoroughly explained in section 2.4 of present study .

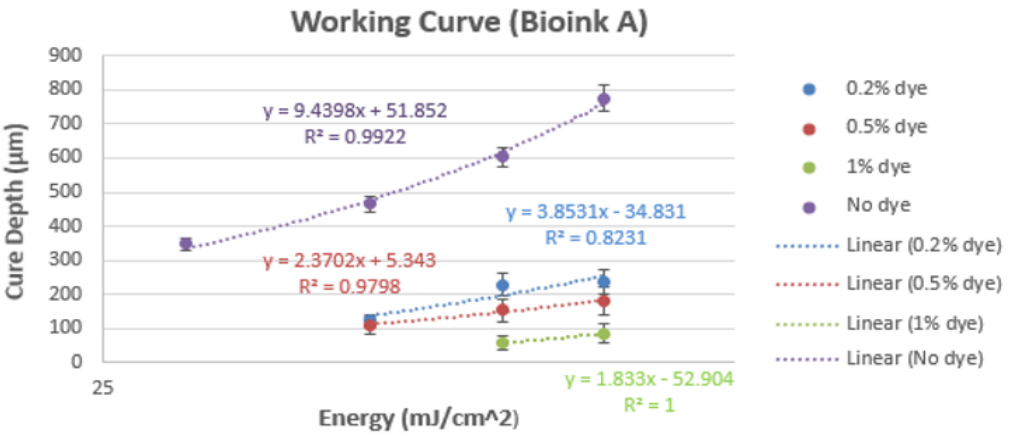

Figure 5.1: Working curves for the bioink A with 10% GelMA fish + 0.2% LAP + Different yellow dye concentrations varying from 0 to 0.2%, 0.5% and 1% using the Atum 3D printer.

From the working curves created for the Bioink A (**Figure 5.1**) and the corresponding trendlines, the Ec for the bioresin without any photoabsorber (dye) is 3.76 mJ/cm^2, while for the other formulations with 0.2%, 0.5% and 1% dye were 4.06, 3.7 and 4.84 mJ/cm^2, respectively. It is observed that the addition of dye reduces the light penetration depth ($Dp = a$ =slope) allowing better control over the printing resolution.

Based on the constructed working curves, the optimal printing parameters can be selected, taking under consideration a general rule of thumb, according to which the cure depth should be approximately double of the layer thickness (i.e step increment of the printer). This ensures that two subsequent layers will be attached to each other during the layer-by-layer printing of a construct. In order to test the printing resolution of the Atum 3D printer, a simple computer-aided (CAD) design of a 3x3 mm tube with 1 mm diameter channel was attempted to be printed.

Based on the final working curve (**Figure 5.1**) and the aforementioned rule of thumb, the following trials of printing the tube were performed:
- 1st Trial: Resin with 10% GelMA fish + 0.2% LAP + 0.5% dye

Printing job properties: 0.050 mm layer thickness and 80% light intensity
- 2nd Trial: Resin with 10% GelMA fish + 0.2% LAP + 0.5% dye
Printing job properties: 0.050 mm layer thickness and 100% light intensity
- 3rd Trial: Resin with 10% GelMA fish + 0.2% LAP + 0.2% dye
Printing job properties: 0.075 mm layer thickness and 60% light intensity
- 4th Trial: Resin with 10% GelMA fish + 0.2% LAP + 0.2% dye
Printing job properties: 0.075 mm layer thickness and 100% light intensity

In all the trials no cube was printed. It was speculated that this issue could be attributed to the inadequate crosslinking efficiency of GelMA due to a possible defective synthesis, since not the same batch of GelMA was used for the construction of the working curves and the printing trials of the cube model.

Preliminary Test 2

- Printer: Perfactory 3 Mini EnvisionTEC.
- Tested bioink B: 5% GelMA + 5% Gelatin + 0.8% PEO + 2/20 mM ru/SPS + Different red dye concentrations varying from 0 to 1% and 2% (*)
- Tested bioink C: 10% GelMA + 10% Gelatin + 1.6% PEO + 2/20 mM ru/SPS + Two different red dye concentrations, 0 and 1% (*)

  * The ru/SPS combination of photoinitiators constitutes a promising system for the fabrication of cell-laden constructs with high shape accuracy and prolonged cell viability, since it minimizes the oxygen inhibition phenomenon and uses visible light instead of UV, that has improved cell cytocompatibility [76,77].
  The PEO Poly(ethylene oxide) refers to Polyethylene glycol (PEG) with average molecular weight $Mn = 100.000$.

- Working curves: Since the time exposure in the case of the Perfactory printer is fixed to 10 sec by default and the light intensity can be chosen at a specific value, a computer aided-design (CAD) model of 6 discs with 4 mm diameter and different heights was created. The height of each disc was increased by a 50 μm step increment, increasing in this way the time exposure of each disc by 10 sec. The multiplication of light intensity chosen at 4 mW/cm^2 with the time exposure for each disc gave as a result the energy exposure for each disc. The plot of the measured thicknesses (Cure depth, Cd) of

the obtained discs with their corresponding energy exposure resulted in the construction of working curves (**Figures 5.2 and 5.3**).

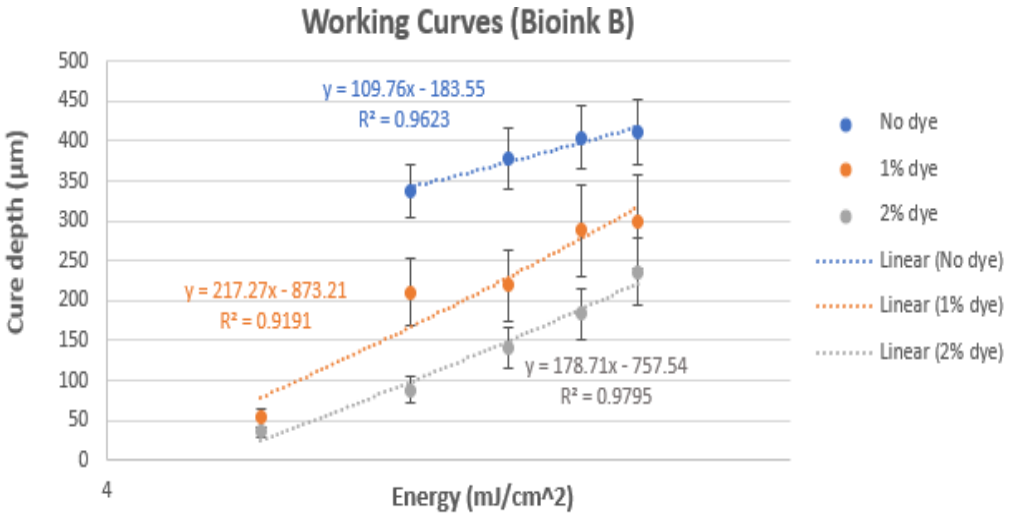

Figure 5.2: Working curves for the bioink B with 5% GelMA + 5% Gelatin + 0.8% PEO + 2/20 mM ru/SPS + Different concentrations of red dye varying from 0 to 1% and 2% using the Perfactory 3 Mini EnvisionTEC.

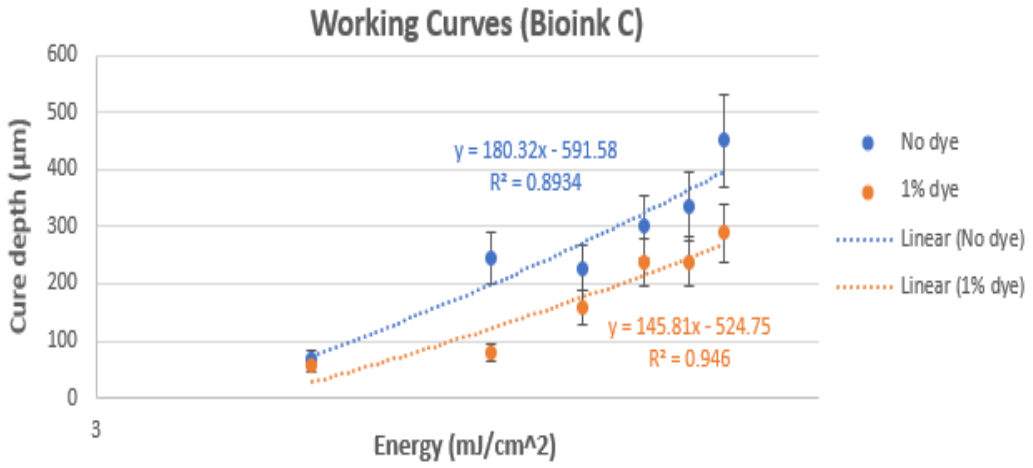

Figure 5.3: Working curves for the bioink C with 10% GelMA + 10% Gelatin + 1.6% PEO + 2/20 mM ru/SPS + Two different concentrations of red dye, 0 and 1% using the Perfactory 3 Mini EnvisionTEC.

From Figures 5.2 and 5.3, it can be generally observed that each curve, individually, presents a logic trendline, since higher the energy exposure, higher should be the thickness/cure depth of each disc for a specific resin.

However, it is expected that the addition of a photoabsorber (dye) should reduce the light penetration depth (Dp), and this is not the case for the working curves corresponding to bioink B, since the addition of more dye seems to increase that light penetration depth, which corresponds to the slope of each trendline, as it has been earlier explained. At this point no further printing trials were performed, since the GelMA used for the resins' formulation was from the same batch which had previously produced unsuccessful results with the Atum3D printer. It was speculated that this GelMA was problematic and the experiments for the DLP printing optimization should be repeated after the synthesis of fresh one with efficient crosslinking properties.

After the preliminary experiments completion, the addition of PEGDA to the final synthesis of an optimal bioresin was decided. It was hypothesized that the addition of this component could improve the mechanical properties of the resultant hydrogels, demonstrating proportionally increased compressive modulus with the concentration of PEGDA. The idea behind the choice of each component for the final bioresin has been thoroughly described in the section 4.1.

Despite the fact that the results of the preliminary experiments were not used for the final thesis project, they demonstrate the complexity of developing a bioink and optimizing its printing resolution. It is worth mentioning that the aforementioned experiments were performed during November and December. Consequently, the printing problems could be related, either with the problematic GelMA, as it has been speculated, or the cold environmental conditions in the laboratory.

A2. Tables with data for development of working curves

The following tables include the data for the development of the working curves for three different PEGDA concentrations. The sample name describes the printing conditions, since the first number indicates the light intensity (100%, 90%, 80%), while the second number indicates the time exposure (from 2 up to 4 sec). According to the printer specifications, the 100% light intensity corresponds the 15 mW/cm^2, while the energy is calculated from the multiplication of the light intensity with the corresponding time exposure. The values of cure depth (μm) correspond to the measured gels' thickness (μm).

5% PEGDA					Cure depth (µm)			
	Sample Name	Time (sec)	Intensity (mW/cm^2)	Energy (mJ/cm^2)	Gel 1	Gel 2	Gel 3	Gel 4
2% Yellow Dye	100-2	2	15	30	80.16798	62.5419	120.1592	109.6523
	90-2	2	13.5	27	52.89482	32.5894	29.1452	58.6391
	100-3	3	15	45	124.5222	142.6854	112.3652	131.0366
	90-3	3	13.5	40.5	107.5355	91.3256	127.9974	87.36524
	80-3	3	12	36	99.13651	87.23661	111.3652	77.965
	100-4	4	15	60	217.3831	251.9841	245.6985	207.362
	90-4	4	13.5	54	187.7035	152.36641	169.3254	198.7452
	80-4	4	12	48	145.7557	125.58712	132.1589	159.1254
2.5% Yellow Dye	100-2	2	15	30	50.73566	62.45123	48.2146	71.2561
	100-3	3	15	45	103.865	91.1225	121.6254	132.1451
	90-3	3	13.5	40.5	80.00477	90.1452	102.5417	72.4587
	80-3	3	12	36	69.51234	52.14521	78.21457	57.14281
	100-4	4	15	60	146.5959	152.32147	168.1259	136.1255
	90-4	4	13.5	54	125.5959	138.36528	141.2681	119.7458
	80-4	4	12	48	112.0186	91.2361	120.8745	89.28741
2.7% Yellow Dye	100-2	2	15	30	21.12548	18.254178	31.87149	12.78541
	100-3	3	15	45	47.25414	51.784512	38.14583	31.25417
	90-3	3	13.5	40.5	34.23652	21.874521	45.48721	37.89541
	80-3	3	12	36	19.25641	18.62147	35.41258	41.84521
	100-4	4	15	60	65.25615	101.84512	81.65214	67.12547
	90-4	4	13.5	54	41.25168	35.47851	52.64713	48.65214
	80-4	4	12	48	29.23651	22.48751	21.5781	45.23659

Figure 5.4: Data table with the printing conditions and the corresponding cure depths for four different gels ($n = 4$) created from the bioink with 5% PEGDA.

10% PEGDA					Cure depth (µm)			
	Sample Name	Time (sec)	Intensity (mW/cm^2)	Energy (mJ/cm^2)	Gel 1	Gel 2	Gel 3	Gel 4
2% Yellow Dye	100-2	2	15	30	106.6099	120.5479	115.3258	135.21
	90-2	2	13.5	27	87.89821	108.2641	78.1478	102.478
	80-2	2	12	24	71.10446	55.7845	84.2145	91.2541
	100-3	3	15	45	165.1596	152.4781	149.5471	179.2541
	80-3	3	12	36	129.9945	145.268	152.7448	134.8954
	100-4	4	15	60	235.4165	258.4417	256.9742	248.9655
2.5% Yellow Dye	100-2	2	15	30	79.47794	68.2175	98.1241	82.1451
	90-2	2	13.5	27	63.97249	74.2145	88.1254	55.1254
	80-2	2	12	24	35.55223	42.547	58.1241	39.124
	100-3	3	15	45	136.9945	152.451	145.3362	116.2478
	80-3	3	12	36	95.60422	82.2158	125.3652	114.541
	100-4	4	15	60	185.4517	225.1251	198.7452	211.487
2.7% Yellow Dye	100-2	2	15	30	53.35047	68.4581	72.5487	49.21478
	90-2	2	13.5	27	36.16981	47.4517	32.4871	50.1496
	80-2	2	12	24	26.31829	22.5129	32.8947	41.2358
	100-3	3	15	45	117.0284	105.147	132.5421	124.6398
	90-3	3	13.5	40.5	108.4618	97.2184	119.5487	98.6521
	80-3	3	12	36	83.19056	78.2177	97.2641	101.5471
	100-4	4	15	60	147.6889	138.1274	158.6128	162.3241
	90-4	4	13.5	54	131.9366	145.3621	127.3652	118.3254
	80-4	4	12	48	112.7337	123.1452	105.1225	99.23871

Figure 5.5: Data table with the printing conditions and the corresponding cure depths for four different gels ($n = 4$) created from the bioink with 10% PEGDA.

15% PEGDA					Cure depth (µm)			
	Sample Name	Time (sec)	Intensity (mW/cm^2)	Energy (mJ/cm^2)	Gel 1	Gel 2	Gel 3	Gel 4
2.7% Yellow Dye	100-2	2	15	30	111.7234	132.2541	128.4512	109.2145
	90-2	2	13.5	27	78.45124	80.2564	75.26541	100.2546
	80-2	2	12	24	74.14587	68.214	80.24613	97.26547
	100-3	3	15	45	194.4543	185.47951	201.4875	281.4579
	90-3	3	13.5	40.5	152.5038	148.2654	132.5478	160.3567
	80-3	3	12	36	121.9556	150.245	122.487	130.7481
2.8% Yellow Dye	100-2	2	15	30	38.32046	45.12459	42.12512	31.12547
	90-2	2	13.5	27	27.31574	38.124574	31.48751	26.42125
	100-3	3	15	45	77.74265	65.147845	57.41255	62.14578
	90-3	3	13.5	40.5	56.41517	42.124871	39.45127	51.12478
	80-3	3	12	36	31.93749	25.2115	34.12548	28.78451

Figure 5.6: Data table with the printing conditions and the corresponding cure depths for four different gels ($n = 4$) created from the bioink with 15% PEGDA.

A3. Trials to fix the problem with Atum3D printer

During the conduction of the present thesis project and after the successful printing optimization of two bioinks (with 10% and 15% PEGDA), the printer stopped to fabricate well-defined prints. Particularly, even though the exact same previously optimized bioinks and printing properties were used, only incomplete prints were fabricated due to their detachment from the building plate. In order to resolve this problem, all the possible parameters which could affect the printing process were examined and classified into three groups: the parameters related with he printer itself, the synthesis of the bioink, and the environmental conditions in the laboratory.

In order to investigate if the problem was related with the printer, the building plate, as well as the resin basin (VAT) were checked for any defects. Moreover, diagnostic tests and the calibration of the printer were performed, but no sign of malfunction was discovered. Finally, the successful printing of structures using the available commercial resins indicated that the problem was not related with printer, but probably with the developed bioresins.

For this reason the bioresins' synthesis, as well as, the corresponding printing parameters should be re-evaluated. **Figure 5.7** demonstrates what kind of parameters need to be set on the printer's software, while **Figure 5.8** shows the conditions for the originally optimized bioinks.

a

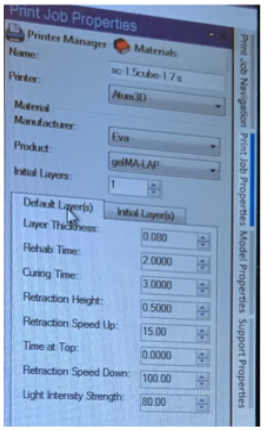

b

- **Initial Layers**: Amount of initial layers. These layers will be used to fix the print job on the build platform.
- **Layer Thickness**: The layer thickness (in mm)
- **Rehab Time**: The time needed for the material to be levelled (in seconds)
- **Curing Time**: The time need for the material to cure (in seconds)
- **Retraction Height**: The amount of retraction that is needed for the material to be released from the VAT (in mm)
- **Retraction Speed Up**: The speed for the up retraction (in mm per minute)
- **Time at Top**: The time required for the material to be levelled (in seconds)
- **Retraction Speed Down**: The speed for the down retraction (in mm per minute)
- **Light Intensity Strength**: Intensity of light in %, where 100% corresponds to 15 mW/cm ^{2}

Figure 5.7: (a) Print Job Properties panel of Atum3D Operator Station software, which gives access to the DLP Station Manager and the Materials database. (b) Description of printing parameters (same for default and initial layers).

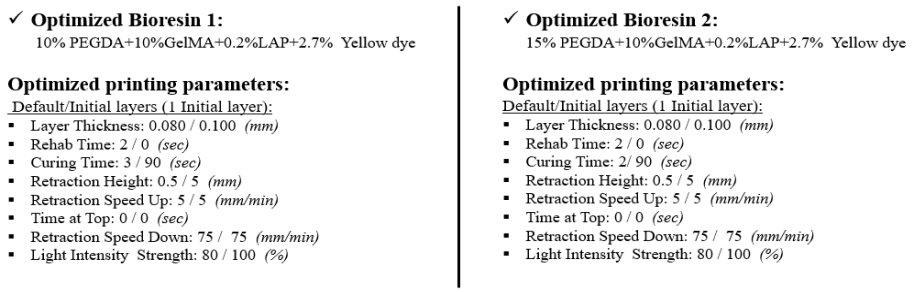

Figure 5.8: Characteristics of originally optimized bioinks (with 10% and 15% PEGDA) in terms of synthesis and printing parameters.

Since the actual problem of the printing process was related with the detachment of the prints from the building plate during the fabrication process, all the performed trials were focusing on increasing the crosslinking efficiency of the bioinks. For all trials the same design, as it has been described in the present thesis, was used, in order to have the same reference in terms of resolution. The following list of trials describes only the conditions that were changed each time, while the rest were considered the same. The symbol ”Pe” refers to ”Personal” batch of GelMA, while ”B09” and ”B08” to other available at the lab batches of GelMA.

- Trial 1: Bioresin 1/Pe - Reduce layer thickness from 80 to 70 μm (Fail)

- Trial 2: Bioresin 1/Pe - Reduce layer thickness from 80 to 60 μm (Fail)

- Trial 3: Bioresin 1/Pe - Increase number of initial layers from 1 to 2 (Fail)

- Trial 4: Bioresin 1/Pe - Decrease dye concentration from 2.7% to 2.5% dye + Increase curing time of initial layer from 90 to 100 sec+ Increase light intensity from 80% to 85% (Fail)

- Trial 5: Bioresin 2/Pe - Increase curing time of initial layer from 90 to 100 sec + Increase light intensity from 80% to 90% + Increase system’s temperature (Pre-warm solutions, hairdryer, beakers with hot water) (Fail)

- Trial 6: Bioresin 1/Pe - Increase number of initial layers from 1 to 2 + Increase curing time of initial layers from 90 to 120 sec + Increase system's temperature (Fail)

- Trial 7: Bioresin 1/Pe - Increase number of initial layers from 1 to 3 + Increase curing time of initial layers from 90 to 100 sec + Decrease dye concentration from 2.7% to 2% + Increase system's temperature (Fail)

- **Trial 8**: Bioresin 1/Pe - Decrease dye concentration from 2.7% to 1% + Increase retraction height from 0.5 to 2 mm + Increase system's temperature (**Success**)
  Conclusions: The dye concentration and the retraction height affect significantly the printing process and they have to be re-optimized. The temperature was kept increased up to $\approx 26^{\circ}$ for the rest of the trials

- Trial 9: Bioresin 1/Pe - Increase dye concentration to 2.7% (optimal) + Keep retraction height to 2 mm (Fail)

- Trial 10: Bioresin 1/Pe - Decrease dye concentration from 2.7% (optimal) to 1% + Reduce retraction height from 2 to 0.5 mm (Fail)

- Trial 11: Bioresin 1/Pe - Reduce dye concentration from 2.7% to 1% + Reduce retraction height from 2 to 0.5 mm (Fail)

- Trial 12: Bioresin 1/Pe - Reduce dye concentration from 2.7% to 1.5% + Increase retraction height from 0.5 to 1 mm (Fail)

- **Trial 13**: Bioresin 1/Pe - Reduce dye concentration from 1.5% to 1% + Increase retraction height from 1 to 2 mm (**Success**)

- **Trial 14**: Bioresin 1/Pe - Increase dye concentration from 1% to 1.2% + Reduce retraction height 2 to 1 mm (**Success/Mediocre resolution**)

- Trial 15: Bioresin 1/Pe - Keep dye concentration to 1.2% + Reduce retraction height from 1 to 0.5 mm (Fail)
  Conclusion: Keep retraction height to 1 mm for the rest of the trials

- **Trial 16**: Bioresin 2/Pe - Keep dye concentration to 1.2% + Keep retraction height to 1 mm (**Success-Bad resolution**)

The Trials 14 and 16 produced complete structures for the bioinks with 10% and 15% PEGDA, correspondingly, with the highest so far dye concentration (1.2%). The following trials were performed in an effort to maximize the printing resolution.

For resolution optimization of Bioink 1:

- Trial 17: Bioresin 1/Pe - Increase dye concentration from 1.2% to 1.7% (Fail)

- Trial 18: Bioresin 1/B08 - Increase dye concentration from 1.2% to 1.7% (Fail)

- Trial 19: Bioresin 1/B09 - Increase dye concentration from 1.2% to 1.7% (Fail)

- **Trial 20**: Bioresin 1/Pe - Decrease dye concentration from 1.7% to 1.1% (**Success**)

- Trial 21: Bioresin 1/Pe - Decrease dye concentration from 1.7% to 1.4% (Fail)

- Trial 22: Bioresin 1/Pe - Decrease dye concentration from 1.7% to 1.3% (Fail)
  Conclusion: Keep the dye concentration 1.2% as optimal in terms of resolution for Bioink 1 (10% PEGDA).

For resolution optimization of Bioink 2:

- **Trial 23**: Bioresin 2/Pe - Increase dye concentration from 1.2% to 1.4% (**Success-Mediocre resolution**)

- Trial 24: Bioresin 2/Pe - Increase dye concentration from 1.2% to 1.6% (Fail)

- Trial 25: Bioresin 2/Pe - Increase dye concentration from 1.2% to 1.5% (Fail)
  Conclusion: Keep the dye concentration 1.4% as optimal in terms of resolution for Bioink 2 (15% PEGDA).

Bibliography

[1] Baroli, B., 2007. Hydrogels for tissue engineering and delivery of tissueinducing substances. Journal of pharmaceutical sciences, 96(9), pp.21972223.

[2] Groll,J.,Boland,T.,Blunk,T.,Burdick,J.A.,Cho,D.W.,Dalton,P.D.,Derby, B., Forgacs, G., Li, Q., Mironov, V.A. and Moroni, L., 2016. Biofabrication: reappraising the definition of an evolving field. Biofabrication, 8(1), p.013001.

[3] Schubert, C., Van Langeveld, M.C. and Donoso, L.A., 2014. Innovations in 3D printing: a 3D overview from optics to organs. British Journal of Ophthalmology, 98(2), pp.159-161.

[4] Mironov, V., Reis, N. and Derby, B., 2006. Bioprinting: A beginning. Tissue engineering, 12(4), pp.631-634.

[5] Kolesky, D.B., Truby, R.L., Gladman, A.S., Busbee, T.A., Homan, K.A. and Lewis, J.A., 2014. 3D bioprinting of vascularized, heterogeneous cell-laden tissue constructs. Advanced materials, 26(19), pp.3124-3130.

[6] Pati, F., Gantelius, J. and Svahn, H.A., 2016. 3D bioprinting of tissue/organ models. Angewandte Chemie International Edition, 55(15), pp.4650-4665.

[7] Murphy, S.V. and Atala, A., 2014. 3D bioprinting of tissues and organs. Nature biotechnology, 32(8), p.773.

[8] Jiang, J., Carlson, M.A., Teusink, M.J., Wang, H., MacEwan, M.R. and Xie, J., 2015. Expanding two-dimensional electrospun nanofiber membranes in the third dimension by a modified gas-foaming technique. ACS Biomaterials Science & Engineering, 1(10), pp.991-1001.

[9] Bajaj, P., Schweller, R.M., Khademhosseini, A., West, J.L. and Bashir, R., 2014. 3D biofabrication strategies for tissue engineering and regenerative medicine. Annual review of biomedical engineering, 16, pp.247-276.

[10] Goldstein, A.S., Zhu, G., Morris, G.E., Meszlenyi, R.K. and Mikos, A.G., 1999. Effect of osteoblastic culture conditions on the structure of poly (DL-lactic-co-glycolic acid) foam scaffolds. Tissue engineering, 5(5), pp.421-433.

[11] Gong, Y., Ma, Z., Zhou, Q., Li, J., Gao, C. and Shen, J., 2008. Poly (lactic acid) scaffold fabricated by gelatin particle leaching has good biocompatibility for chondrogenesis. Journal of Biomaterials Science, Polymer Edition, 19(2), pp.207-221.

[12] Lo, H., Ponticiello, M.S. and Leong, K.W., 1995. Fabrication of controlled release biodegradable foams by phase separation. Tissue engineering, 1(1), pp.15-28.

[13] Van de Witte, P., Dijkstra, P.J., Van den Berg, J.W.A. and Feijen, J., 1996. Phase separation processes in polymer solutions in relation to membrane formation. Journal of membrane science, 117(1-2), pp.1-31.

[14] Lee, M.K., Rich, M.H., Lee, J. and Kong, H., 2015. A bio-inspired, microchanneled hydrogel with controlled spacing of cell adhesion ligands regulates 3D spatial organization of cells and tissue. Biomaterials, 58, pp.26-34.

[15] Fong, E.L.S., Lamhamedi-Cherradi, S.E., Burdett, E., Ramamoorthy, V., Lazar, A.J., Kasper, F.K., Farach-Carson, M.C., Vishwamitra, D., Demicco, E.G., Menegaz, B.A. and Amin, H.M., 2013. Modeling Ewing sarcoma tumors in vitro with 3D scaffolds. Proceedings of the National Academy of Sciences, 110(16), pp.6500-6505.

[16] Hribar, K.C., Soman, P., Warner, J., Chung, P. and Chen, S., 2014. Light-assisted direct-write of 3D functional biomaterials. Lab on a chip, 14(2), pp.268-275.

[17] Gudapati, H., Dey, M. and Ozbolat, I., 2016. A comprehensive review on droplet-based bioprinting: past, present and future. Biomaterials, 102, pp.20-42.

[18] Wilson Jr, W.C. and Boland, T., 2003. Cell and organ printing 1: protein and cell printers. The Anatomical Record Part A: discoveries in molecular, cellular, and evolutionary biology, 272(2), pp.491-496.

[19] Chang, R., Nam, J. and Sun, W., 2008. Effects of dispensing pressure and nozzle diameter on cell survival from solid freeform fabrication–based direct cell writing. Tissue Engineering Part A, 14(1), pp.41-48.

[20] Bohandy, J., Kim, B.F. and Adrian, F.J., 1986. Metal deposition from a supported metal film using an excimer laser. Journal of Applied Physics, 60(4), pp.1538-1539.

[21] Koch, L., Brandt, O., Deiwick, A. and Chichkov, B., 2017. Laser-assisted bioprinting at different wavelengths and pulse durations with a metal dynamic release layer: A parametric study. International Journal of Bioprinting 3 (2017), Nr. 1, 3(1), pp.42-53.

[22] Mandrycky, C., Wang, Z., Kim, K. and Kim, D.H., 2016. 3D bioprinting for engineering complex tissues. Biotechnology advances, 34(4), pp.422-434.

[23] Malda, J., Visser, J., Melchels, F.P., Jüngst, T., Hennink, W.E., Dhert, W.J., Groll, J. and Hutmacher, D.W., 2013. 25th anniversary article: engineering hydrogels for biofabrication. Advanced materials, 25(36), pp.5011-5028.

[24] Gibson, I. and Rosen, D.W., 2015. Stucker B (2010) additive manufacturing technologies: 3D printing, rapid prototyping, and direct digital manufacturing.

[25] Bagheri, A. and Jin, J., 2019. Photopolymerization in 3D Printing. ACS Applied Polymer Materials, 1(4), pp.593-611.

[26] Gross, B.C., Erkal, J.L., Lockwood, S.Y., Chen, C. and Spence, D.M., 2014. Evaluation of 3D printing and its potential impact on biotechnology and the chemical sciences.

[27] Billiet, T., Vandenhaute, M., Schelfhout, J., Van Vlierberghe, S. and Dubruel, P., 2012. A review of trends and limitations in hydrogel-rapid prototyping for tissue engineering. Biomaterials, 33(26), pp.6020-6041.

[28] Lambert, P.M., Campaigne III, E.A. and Williams, C.B., 2013. Design considerations for mask projection microstereolithography systems. In Solid Freeform Fabrication Symposium, Austin, TX, Aug (pp. 12-14).

[29] Liska, R., Schuster, M., InfŘhr, R., Turecek, C., Fritscher, C., Seidl, B., Schmidt, V., Kuna, L., Haase, A., Varga, F. and Lichtenegger, H., 2007.

Photopolymers for rapid prototyping. Journal of Coatings Technology and Research, 4(4), pp.505-510.

[30] Wu, S., Serbin, J. and Gu, M., 2006. Two-photon polymerisation for three-dimensional micro-fabrication. Journal of Photochemistry and Photobiology A: Chemistry, 181(1), pp.1-11.

[31] Xing, J.F., Zheng, M.L. and Duan, X.M., 2015. Two-photon polymerization microfabrication of hydrogels: an advanced 3D printing technology for tissue engineering and drug delivery. Chemical Society Reviews, 44(15), pp.5031-5039.

[32] Park, S.H., Yang, D.Y. and Lee, K.S., 2009. Two-photon stereolithography for realizing ultraprecise three-dimensional nano/microdevices. Laser & Photonics Reviews, 3(1-2), pp.1-11.

[33] Shi, W., He, R. and Liu, Y., 2015. 3D printing scaffolds with hydrogel materials for biomedical applications. European Journal of BioMedical Research, 1(3), pp.3-8.

[34] Tibbitt, M.W. and Anseth, K.S., 2009. Hydrogels as extracellular matrix mimics for 3D cell culture. Biotechnology and bioengineering, 103(4), pp.655-663.

[35] Hoffman, A.S., 2012. Hydrogels for biomedical applications. Advanced drug delivery reviews, 64, pp.18-23.

[36] Fong, E.L.S., Lamhamedi-Cherradi, S.E., Burdett, E., Ramamoorthy, V., Lazar, A.J., Kasper, F.K., Farach-Carson, M.C., Vishwamitra, D., Demicco, E.G., Menegaz, B.A. and Amin, H.M., 2013. Modeling Ewing sarcoma tumors in vitro with 3D scaffolds. Proceedings of the National Academy of Sciences, 110(16), pp.6500-6505.

[37] Murphy, S.V. and Atala, A., 2014. 3D bioprinting of tissues and organs. Nature biotechnology, 32(8), p.773.

[38] Murphy, Sean V., Aleksander Skardal, and Anthony Atala. "Evaluation of hydrogels for bio-printing applications." Journal of Biomedical Materials Research Part A 101.1 (2013): 272-284.

[39] Skardal, Aleksander, and Anthony Atala. "Biomaterials for integration with 3-D bioprinting." Annals of biomedical engineering 43.3 (2015): 730-746.

[40] Pati, Falguni, et al. ”Biomimetic 3D tissue printing for soft tissue regeneration.” Biomaterials 62 (2015): 164-175.

[41] Shi, Wentao, Ran He, and Yaling Liu. ”3D printing scaffolds with hydrogel materials for biomedical applications.” European Journal of BioMedical Research 1.3 (2015): 3-8.

[42] Lim, K.S., Levato, R., Costa, P.F., Castilho, M.D., Alcala-Orozco, C.R., van Dorenmalen, K.M., Melchels, F.P., Gawlitta, D., Hooper, G.J., Malda, J. and Woodfield, T.B., 2018. Bio-resin for high resolution lithography-based biofabricationofcomplexcell-ladenconstructs.Biofabrication,10(3),p.034101.

[43] Kufelt, O., El-Tamer, A., Sehring, C., Schlie-Wolter, S. and Chichkov, B.N., 2014. Hyaluronic acid based materials for scaffolding via two-photon polymerization. Biomacromolecules, 15(2), pp.650-659.

[44] Mapili, G., Lu, Y., Chen, S. and Roy, K., 2005. Laser-layered microfabrication of spatially patterned functionalized tissue-engineering scaffolds. Journal of Biomedical Materials Research Part B: Applied Biomaterials: An Official Journal of The Society for Biomaterials, The Japanese Society for Biomaterials, and The Australian Society for Biomaterials and the Korean Society for Biomaterials, 75(2), pp.414-424.

[45] Castro, N.J., O'Brien, J. and Zhang, L.G., 2015. Integrating biologically inspired nanomaterials and table-top stereolithography for 3D printed biomimetic osteochondral scaffolds. Nanoscale, 7(33), pp.14010-14022.

[46] Nichol, J.W., Koshy, S.T., Bae, H., Hwang, C.M., Yamanlar, S. and Khademhosseini, A., 2010. Cell-laden microengineered gelatin methacrylate hydrogels. Biomaterials, 31(21), pp.5536-5544.

[47] Pepelanova, I., Kruppa, K., Scheper, T. and Lavrentieva, A., 2018. Gelatin-Methacryloyl (GelMA) hydrogels with defined degree of functionalization as a versatile toolkit for 3D cell culture and extrusion bioprinting. Bioengineering, 5(3), p.55.

[48] Cha, C., Kim, S.Y., Cao, L. and Kong, H., 2010. Decoupled control of stiffness and permeability with a cell-encapsulating poly (ethylene glycol) dimethacrylate hydrogel. Biomaterials, 31(18), pp.4864-4871.

[49] Seeto, W.J., Tian, Y. and Lipke, E.A., 2013. Peptide-grafted poly (ethylene glycol) hydrogels support dynamic adhesion of endothelial progenitor cells. Acta biomaterialia, 9(9), pp.8279-8289.

[50] Compaan, A.M., Christensen, K. and Huang, Y., 2016. Inkjet bioprinting of 3D silk fibroin cellular constructs using sacrificial alginate. ACS Biomaterials Science & Engineering, 3(8), pp.1519-1526.

[51] Bertassoni, L.E., Cecconi, M., Manoharan, V., Nikkhah, M., Hjortnaes, J., Cristino, A.L., Barabaschi, G., Demarchi, D., Dokmeci, M.R., Yang, Y. and Khademhosseini, A., 2014. Hydrogel bioprinted microchannel networks for vascularization of tissue engineering constructs. Lab on a Chip, 14(13), pp.2202-2211.

[52] Suntornnond, R., An, J. and Chua, C.K., 2017. Roles of support materials in 3D bioprinting.

[53] https://www.3dprintingmedia.network/mitsubishi-chemical-and-atum3d-diabeamtm-uv-resin/

[54] Atkins, P. and de Paula, J., 2005. Elements of physical chemistry , W. H.

[55] Jacobs, P.F., 1992. Rapid prototyping & manufacturing: fundamentals of stereolithography. Society of Manufacturing Engineers.

[56] Zhang, R. and Larsen, N.B., 2017. Stereolithographic hydrogel printing of 3D culture chips with biofunctionalized complex 3D perfusion networks. Lab on a Chip, 17(24), pp.4273-4282.

[57] Canal, T. and Peppas, N.A., 1989. Correlation between mesh size and equilibrium degree of swelling of polymeric networks. Journal of biomedical materials research, 23(10), pp.1183-1193.

[58] Roberts, J.J., Naudiyal, P., Lim, K.S., Poole-Warren, L.A. and Martens, P.J., 2016. A comparative study of enzyme initiators for crosslinking phenol-functionalized hydrogels for cell encapsulation. Biomaterials research, 20(1), p.30.

[59] Loh, Q.L. and Choong, C., 2013. Three-dimensional scaffolds for tissue engineering applications: role of porosity and pore size. Tissue Engineering Part B: Reviews, 19(6), pp.485-502.

[60] Grosberg, A., Alford, P.W., McCain, M.L. and Parker, K.K., 2011. Ensembles of engineered cardiac tissues for physiological and pharmacological study: heart on a chip. Lab on a chip, 11(24), pp.4165-4173.

[61] Magnusson, M.K. and Mosher, D.F., 1998. Fibronectin: structure, assembly, and cardiovascular implications. Arteriosclerosis, thrombosis, and vascular biology, 18(9), pp.1363-1370.

[62] Cooper, T.P. and Sefton, M.V., 2011. Fibronectin coating of collagen modules increases in vivo HUVEC survival and vessel formation in SCID mice. Acta biomaterialia, 7(3), pp.1072-1083.

[63] Yue, K., Trujillo-de Santiago, G., Alvarez, M.M., Tamayol, A., Annabi, N. and Khademhosseini, A., 2015. Synthesis, properties, and biomedical applications of gelatin methacryloyl (GelMA) hydrogels. Biomaterials, 73, pp.254-271.

[64] Nichol, J.W., Koshy, S.T., Bae, H., Hwang, C.M., Yamanlar, S. and Khademhosseini, A., 2010. Cell-laden microengineered gelatin methacrylate hydrogels. Biomaterials, 31(21), pp.5536-5544.

[65] Rose, J., Pacelli, S., Haj, A., Dua, H., Hopkinson, A., White, L. and Rose, F., 2014. Gelatin-based materials in ocular tissue engineering. Materials, 7(4), pp.3106-3135.

[66] Somboon, N., Karrila, T.T., Kaewmanee, T. and Karrila, S.J., 2014. Properties of gels from mixed agar and fish gelatin. International Food Research Journal, 21(2).

[67] Koshy, S.T., Ferrante, T.C., Lewin, S.A. and Mooney, D.J., 2014. Injectable, porous, and cell-responsive gelatin cryogels. Biomaterials, 35(8), pp.2477-2487.

[68] Cha, C., Kim, S.Y., Cao, L. and Kong, H., 2010. Decoupled control of stiffness and permeability with a cell-encapsulating poly (ethylene glycol) dimethacrylate hydrogel. Biomaterials, 31(18), pp.4864-4871.

[69] Weber, L.M., Lopez, C.G. and Anseth, K.S., 2009. Effects of PEG hydrogel crosslinking density on protein diffusion and encapsulated islet survival and function. Journal of Biomedical Materials Research Part A: An Official

Journal of The Society for Biomaterials, The Japanese Society for Biomaterials, and The Australian Society for Biomaterials and the Korean Society for Biomaterials, 90(3), pp.720-729.

[70] Mironi-Harpaz, I., Wang, D.Y., Venkatraman, S. and Seliktar, D., 2012. Photopolymerization of cell-encapsulating hydrogels: crosslinking efficiency versus cytotoxicity. Acta biomaterialia, 8(5), pp.1838-1848.

[71] Gong, H., Beauchamp, M., Perry, S., Woolley, A.T. and Nordin, G.P., 2015. Optical approach to resin formulation for 3D printed microfluidics. RSC advances, 5(129), pp.106621-106632.

[72] Gong, H., Bickham, B.P., Woolley, A.T. and Nordin, G.P., 2017. Custom 3D printer and resin for 18 μm× 20 μm microfluidic flow channels. Lab on a Chip, 17(17), pp.2899-2909.

[73] Devegowda, D., Doddamani, P. and Vishwanath, P., 2014. Human papillomavirus screening: Time to add molecular methods with cytology. International Journal of Health & Allied Sciences, 3(3), p.145.

[74] de Gruijl, F.R., van Kranen, H.J. and Mullenders, L.H., 2001. UV-induced DNA damage, repair, mutations and oncogenic pathways in skin cancer. Journal of Photochemistry and Photobiology B: Biology, 63(1-3), pp.19-27.

[75] Nanda, K., McCrory, D.C., Myers, E.R., Bastian, L.A., Hasselblad, V., Hickey, J.D. and Matchar, D.B., 2000. Accuracy of the Papanicolaou test in screening for and follow-up of cervical cytologic abnormalities: a systematic review. Annals of internal medicine, 132(10), pp.810-819.

[76] Lim, K.S., Schon, B.S., Mekhileri, N.V., Brown, G.C., Chia, C.M., Prabakar, S., Hooper, G.J. and Woodfield, T.B., 2016. New visible-light photoinitiating system for improved print fidelity in gelatin-based bioinks. ACS Biomaterials Science & Engineering, 2(10), pp.1752-1762.

[77] Lim, K.S., Levato, R., Costa, P.F., Castilho, M.D., Alcala-Orozco, C.R., van Dorenmalen, K.M., Melchels, F.P., Gawlitta, D., Hooper, G.J., Malda, J. and Woodfield, T.B., 2018. Bio-resin for high resolution lithography-based biofabrication of complex cell-laden constructs. Biofabrication, 10(3), p.034101.

[78] Yue, K., Trujillo-de Santiago, G., Alvarez, M.M., Tamayol, A., Annabi, N. and Khademhosseini, A., 2015. Synthesis, properties, and biomedical applications of gelatin methacryloyl (GelMA) hydrogels. Biomaterials, 73, pp.254-271.

[79] Wang, F., Chong, Y., Wang, F. and He, C., 2017. Photopolymer resins for luminescent three-dimensional printing. Journal of Applied Polymer Science, 134(32), p.44988.

[80] Macdonald, N.P., Cabot, J.M., Smejkal, P., Guijt, R.M., Paull, B. and Breadmore, M.C., 2017. Comparing microfluidic performance of three-dimensional (3D) printing platforms. Analytical chemistry, 89(7), pp.3858-3866.

[81] Nichol, J.W., Koshy, S.T., Bae, H., Hwang, C.M., Yamanlar, S. and Khademhosseini, A., 2010. Cell-laden microengineered gelatin methacrylate hydrogels. Biomaterials, 31(21), pp.5536-5544.

[82] Peppas, N.A., Hilt, J.Z., Khademhosseini, A. and Langer, R., 2006. Hydrogels in biology and medicine: from molecular principles to bionanotechnology. Advanced materials, 18(11), pp.1345-1360.

[83] Chaudhuri, O., Gu, L., Klumpers, D., Darnell, M., Bencherif, S.A., Weaver, J.C., Huebsch, N., Lee, H.P., Lippens, E., Duda, G.N. and Mooney, D.J., 2016. Hydrogels with tunable stress relaxation regulate stem cell fate and activity. Nature materials, 15(3), p.326.

[84] Fung, Y.C., 2013. Biomechanics: mechanical properties of living tissues. Springer Science & Business Media.

[85] Levental, I., Georges, P.C. and Janmey, P.A., 2007. Soft biological materials and their impact on cell function. Soft Matter, 3(3), pp.299-306.

[86] Papanicolaou, G.C. and Zaoutsos, S.P., 2019. Viscoelastic constitutive modeling of creep and stress relaxation in polymers and polymer matrix composites. In Creep and fatigue in polymer matrix composites (pp. 3-59). Woodhead Publishing.

[87] Schmidt, M.B., Mow, V.C., Chun, L.E. and Eyre, D.R., 1990. Effects of proteoglycan extraction on the tensile behavior of articular cartilage. Journal of Orthopaedic Research, 8(3), pp.353-363.

[88] Hayes, W.C. and Mockros, L.F., 1971. Viscoelastic properties of human articular cartilage. Journal of applied physiology, 31(4), pp.562-568.

[89] Torzilli, P.A., Dethmers, D.A., Rose, D.E. and Schryuer, H.F., 1983. Movement of interstitial water through loaded articular cartilage. Journal of biomechanics, 16(3), pp.169-179.

[90] Maroudas, A., 1975. Biophysical chemistry of cartilaginous tissues with special reference to solute and fluid transport. Biorheology, 12(3-4), pp.233-248.

[91] Ateshian, G.A., Warden, W.H., Kim, J.J., Grelsamer, R.P. and Mow, V.C., 1997. Finite deformation biphasic material properties of bovine articular cartilage from confined compression experiments. Journal of biomechanics, 30(11-12), pp.1157-1164.

[92] Mow, V.C., Kuei, S.C., Lai, W.M. and Armstrong, C.G., 1980. Biphasic creep and stress relaxation of articular cartilage in compression: theory and experiments. Journal of biomechanical engineering, 102(1), pp.73-84.

[93] Mak, A.F., Lai, W.M. and Mow, V.C., 1987. Biphasic indentation of articular cartilage—I. Theoretical analysis. Journal of biomechanics, 20(7), pp.703-714.

[94] Mazzoccoli, J.P., Feke, D.L., Baskaran, H. and Pintauro, P.N., 2010. Mechanical and cell viability properties of crosslinked low-and high-molecular weight poly (ethylene glycol) diacrylate blends. Journal of Biomedical Materials Research Part A: An Official Journal of The Society for Biomaterials, The Japanese Society for Biomaterials, and The Australian Society for Biomaterials and the Korean Society for Biomaterials, 93(2), pp.558-566.

[95] Zhang, H., Wang, L., Song, L., Niu, G., Cao, H., Wang, G., Yang, H. and Zhu, S., 2011. Controllable properties and microstructure of hydrogels based on crosslinked poly (ethylene glycol) diacrylates with different molecular weights. Journal of Applied Polymer Science, 121(1), pp.531-540.

[96] Wang, Z., Kumar, H., Tian, Z., Jin, X., Holzman, J.F., Menard, F. and Kim, K., 2018. Visible light photoinitiation of cell-adhesive gelatin methacryloyl hydrogels for stereolithography 3D bioprinting. ACS applied materials & interfaces, 10(32), pp.26859-26869.

[97] Lim, K.S., Schon, B.S., Mekhileri, N.V., Brown, G.C., Chia, C.M., Prabakar, S., Hooper, G.J. and Woodfield, T.B., 2016. New visible-light photoinitiating system for improved print fidelity in gelatin-based bioinks. ACS Biomaterials Science & Engineering, 2(10), pp.1752-1762.

[98] Nichol, J.W., Koshy, S.T., Bae, H., Hwang, C.M., Yamanlar, S. and Khademhosseini, A., 2010. Cell-laden microengineered gelatin methacrylate hydrogels. Biomaterials, 31(21), pp.5536-5544.

[99] Karageorgiou, V. and Kaplan, D., 2005. Porosity of 3D biomaterial scaffolds and osteogenesis. Biomaterials, 26(27), pp.5474-5491.

[100] Hollister, S.J., 2005. Porous scaffold design for tissue engineering. Nature materials, 4(7), p.518.

[101] Woodard, J.R., Hilldore, A.J., Lan, S.K., Park, C.J., Morgan, A.W., Eurell, J.A.C., Clark, S.G., Wheeler, M.B., Jamison, R.D. and Johnson, A.J.W., 2007. The mechanical properties and osteoconductivity of hydroxyapatite bone scaffolds with multi-scale porosity. Biomaterials, 28(1), pp.45-54.